Crystal structures, atomic vibration, and disorder of the type-I thermoelectric clathrates $Ba_8Ga_{16}Si_{30}$, $Ba_8Ga_{16}Ge_{30}$, $Ba_8In_{16}Ge_{30}$, and $Sr_8Ga_{16}Ge_{30}$

A. Bentien,[1] E. Nishibori,[2] S. Paschen,[3] and B. B. Iversen[1,*]
[1]*Department of Chemistry, University of Aarhus, DK-8000 Aarhus C, Denmark*
[2]*Department of Applied Physics, Nagoya University, Nagoya 464-8603, Japan*
[3]*Max Planck Institute for Chemical Physics of Solids, 01187 Dresden, Germany*
(Received 28 June 2004; revised manuscript received 11 November 2004; published 13 April 2005)

Temperature dependent synchrotron powder diffraction and single crystal neutron diffraction data are used for probing the vibrational states and disorder in type I clathrates $Ba_8Ga_{16}Si_{30}$, $Ba_8Ga_{16}Ge_{30}$, $Ba_8In_{16}Ge_{30}$, and $Sr_8Ga_{16}Ge_{30}$. If an empirical disorder term is included, the temperature dependence of the atomic displacement factors (ADPs) of the framework and guest atoms can be described by a Debye and Einstein model, respectively. None of the guest atoms in the large cages are located in the center and the vibrational frequencies (θ_E) are of the order 80 K or larger for all structures, in good agreement with theoretical predictions. Even though the Sr ADPs are larger than the Ba ADPs in all the clathrates, the data show that θ_E of Sr in $Sr_8Ga_{16}Ge_{30}$ is larger than for the Ba atoms. This is due to stronger guest-host chemical bonding in $Sr_8Ga_{16}Ge_{30}$. Since θ_E of Sr has been reported to be much smaller in the literature we have also measured the specific heat of $Sr_8Ga_{16}Ge_{30}$ with $Ba_8Ga_{16}Ge_{30}$ as a reference. It is found that localized excitations with a characteristic energy of approximately 35 K exist in both compounds, however, the total number of states is too low to be associated with either tunneling states or localized vibration of each of the guest atoms.

DOI: 10.1103/PhysRevB.71.144107 PACS number(s): 61.12.−q, 72.15.Jf, 61.66.−f

I. INTRODUCTION

Recently a surge of interest in thermoelectric materials has been caused by the discovery of new promising materials with open framework structures.[1,2] Particular interest has concerned inorganic clathrates, Fig. 1, which have been studied with a plethora of techniques.[3–11] A large number of elemental compositions can form the clathrate type I structure and common to the different compositions is the total number of 184 valence electrons per unit cell. For this reason chemists often regard the clathrates as Zintl phases,[12] where the encapsulated guest atoms donate their valence electrons to the framework. This leads to complete filling of the sp^3 orbitals of the tetrahedrally coordinated framework atoms and the clathrates therefore are expected to be semiconductors. The simple Zintl picture of the clathrates was recently confirmed to be quite accurate by a theoretical charge density analysis study.[13] There are two basic hypotheses for the good thermoelectric properties of the clathrates. First, the semiconducting framework provides a high Seebeck coefficient (S) and electrical conductivity (σ). Second, the acoustic phonons are resonantly scattered from the loosely bound guest atoms[14,15] which leads to a very low thermal conductivity (κ). Together, these properties result in high values of the thermoelectric figure of merit $ZT=S^2\sigma/\kappa T$, where T is the temperature. The conversion efficiency for thermoelectric cooling or power generation increases monotonically with ZT.

The crystal structures of $Ba_8Ga_{16}Si_{30}$, $Ba_8Ga_{16}Ge_{30}$, $Ba_8In_{16}Ge_{30}$, and $Sr_8Ga_{16}Ge_{30}$ have been reported by a number of different authors using varying levels of crystallographic sophistication. Both single crystal and powder diffraction data have been reported, and neutron, conventional x-ray, and synchrotron x-ray diffraction have been used.[6–9,11,16–19] The strong focus on crystal structure determinations of clathrates is due to the fact that subtle structural details such as the exact sitting of dopant atoms (e.g., Ga in Ga/Ge clathrates) or possible structural disorder of the guest atoms can greatly affect the thermoelectric properties.[18] Thus accurate structural information is a prerequisite for any detailed understanding of the physical properties of the sys-

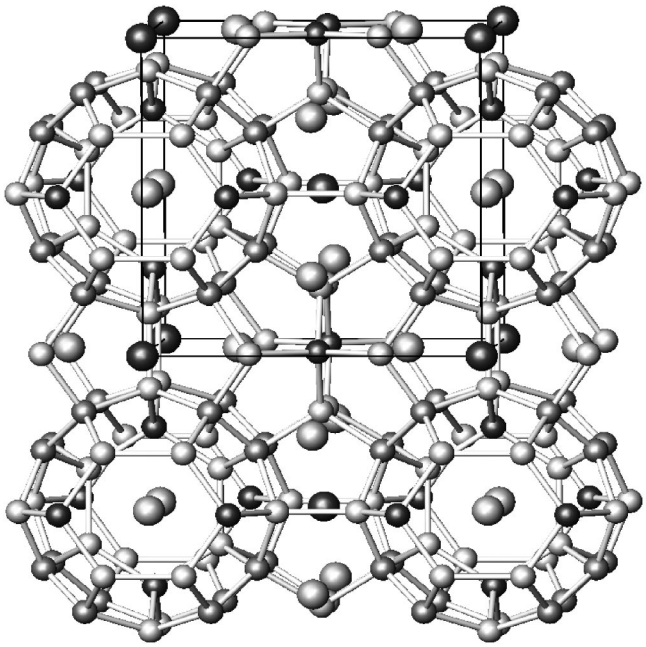

FIG. 1. The clathrate type I structure. The large dark atoms are M1 (Ba/Sr) on the 2*a* site, the large gray atoms M2 (Ba/Sr) on the 6*d* site. The small, black, gray and light gray atoms are Ga/Si/In on the 6*c* (H_{6c}), 16*i* (H_{16i}), and 24*k* (H_{24k}) sites, respectively.

tems. For β-$Eu_8Ga_{16}Ge_{30}$ (Ref. 8) [in the following referred to as $Eu_8Ga_{16}Ge_{30}$ (Ref. 9)] and $Sr_8Ga_{16}Ge_{30}$ (Refs. 8 and 20) it is generally accepted that the guest atom in the large cage (M2) is displaced away from the cage center and disordered over four sites in the (100) plane (24*k* site). At least in the case of $Sr_8Ga_{16}Ge_{30}$ this is a crude approximation. First, modeling of diffraction data with a 24*j* site, which corresponds to a 45° rotation of the split site in the (100) plane, model data equally well.[21,22] Second, fourth-order anharmonic temperature factors can also be used for modeling the disorder.[23] Third, maximum entropy method (MEM) analysis of x-ray diffraction data[7] indicates that the "equilibrium" position is distributed over a surface normal to the (100) plane and shaped like an elongated torus. This also appears to be the case for $Eu_8Ga_{16}Ge_{30}$ where difference Fourier maps, from neutron diffraction, indicate that the Eu equilibrium position in the large cage is doughnut- or torus-shaped.[22] For Ba containing clathrates elaborate crystallographic analysis has been carried out, and based on maximum entropy method (MEM) nuclear density analysis and modeling of atomic displacement parameters (ADP) it was shown that both types of Ba atoms are disordered in the $Ba_8Ga_{16}Si_{30}$ structure.[7,24] However, in the literature it is not always acknowledged that also in Ba containing systems the guest atoms are disordered.[8] This is despite the fact that it is possible to refine x-ray diffraction data with a split site for Ba in the large cage of $Ba_8Ga_{16}Ge_{30}$ (Refs. [9,18]) and $Ba_8Ga_{16}Si_{30}$.[18] One problem with barium containing clathrates has been the interpretation of the low temperature lattice thermal conductivity (κ_L) data of $Ba_8Ga_{16}Ge_{30}$, $Sr_8Ga_{16}Ge_{30}$, and $Eu_8Ga_{16}Ge_{30}$.[8,25] For $Sr_8Ga_{16}Ge_{30}$ and $Eu_8Ga_{16}Ge_{30}$ samples a glasslike κ_L is observed, while *n*-type $Ba_8Ga_{16}Ge_{30}$ has a "normal" crystal-like κ_L. This was interpreted as being related to the lack of structural disorder on the Ba guest atom sites in $Ba_8Ga_{16}Ge_{30}$. However, it was recently discovered that *p*-type $Ba_8Ga_{16}Ge_{30}$ samples, just like $Sr_8Ga_{16}Ge_{30}$ and $Eu_8Ga_{16}Ge_{30}$, have a glass-like κ_L.[26] The thermal conductivity data therefore are not in contradiction with the Ba guest atom disorder revealed in other crystallographic studies.[7,24] Nevertheless, in order to investigate the structural differences between different clathrates in detail, we have decided to reinvestigate the crystal structures of $Ba_8Ga_{16}Si_{30}$, $Ba_8Ga_{16}Ge_{30}$, $Ba_8In_{16}Ge_{30}$, and $Sr_8Ga_{16}Ge_{30}$ using exactly the same technique, multitemperature synchrotron powder diffraction, to minimize systematic errors between the studies. As an example there is up to 80% variation in the framework atomic displacement parameters (ADPs) reported in different studies of $Ba_8Ga_{16}Ge_{30}$ and this makes comparative analysis difficult. Furthermore, analysis of multitemperature diffraction data using the full Debye and Einstein models has never previously been reported. By systematically studying four representative clathrate systems with varying guest atoms (Ba or Sr), dopant atoms (Ga or In), and framework atoms (Si or Ge) it is possible to make a direct comparison of important physical quantities such as θ_E and θ_D with limited influence of systematic errors. It will be shown that the comparative analysis reveals a hitherto unrecognized discrepancy between Raman spectroscopy and heat capacity data on the one hand and theoretical calculations and diffraction data on the other.

The paper is outlined as follows. First, a short summary of the experimental details is given. This is followed by a thorough analysis of the temperature dependence of the framework atomic displacement parameters (ADPs) of $Ba_8Ga_{16}Si_{30}$ obtained from single crystal neutron diffraction.[24] These results are compared with the ones from synchrotron powder diffraction experiments to show that synchrotron powder diffraction can be used as a tool for obtaining accurate crystallographic parameters. The temperature dependence of the ADPs of the four compounds is analyzed in terms of Debye and Einstein models and it will be shown (i) that information about the framework disorder can be extracted, (ii) positional disorder of the guest atoms in the large cage appears to be the rule rather than an exception as is also the case for sodium containing silicon clathrates,[27] and (iii) there is no clear cut distinction between fully ordered and disordered guest atoms, but rather a continuous change between different clathrates. To explore the vibrational states further we also measured the specific heat (C_p) of $Ba_8Ga_{16}Ge_{30}$ and $Sr_8Ga_{16}Ge_{30}$ and compare it to the complementary information from the temperature dependence of the ADPs. Our analysis shows that if tunneling states are present they either have a low total number of states or the energy scale of the excitations is below k_BT of the specific heat measurement. Finally, we show the results of MEM analysis of the multitemperature neutron diffraction data to obtain more unbiased information of the guest atom disorder in $Ba_8Ga_{16}Si_{30}$.

II. EXPERIMENT

A. Single crystal neutron diffraction

Multitemperature single crystal neutron diffraction data were collected on the SCD instrument at the Intense Pulsed Neutron Source, Argonne National Laboratory, during two separate beam time allocations. Analysis of these data focusing on the guest atom motion was reported earlier.[24] Here we briefly repeat the most important experimental details. During the first allocation (two weeks) data were collected at 15, 100, 150, 200, and 300 K, and during the second allocation (two weeks) at 450, 600, and 900 K. The crystal was a rectangular-shaped prism of dimensions $3.8 \times 3.8 \times 2.0$ mm^3 grown by the flux method.[28] For the high temperature measurements the crystal volume had to be slightly reduced to fit inside the furnace. Both sets of measurements were carried out with the crystal wrapped tightly in aluminum foil and fastened on an aluminum pin by tiny amounts of glue, thus avoiding glue directly on the crystal. The SCD instrument employs the white beam of a spallation source, and the diffractometer is equipped with a position sensitive area detector. The instrument uses ω fixed at 45° and different volumes of reciprocal space are recorded by setting ϕ and χ at a number of values. Only neutrons having wavelengths between 0.7 and 4.2 Å were considered as observed. The number of significant reflections is reduced at higher temperatures due to the much increased thermal vibration and the smaller crystal volume. Local Argonne National Laboratory programs were used for the data acquisition, data reduction, and initial structure refinements.[29] The intensities

TABLE I. Experimental details for the neutron data on $Ba_8Ga_{16}Si_{30}$. The internal agreement factor (R_I) is calculated from extinction corrected structure factors. For all data sets $(\sin\theta/\lambda)_{max}$ is approximately 1.1 $Å^{-1}$.

T(K)	a (Å)	V ($Å^3$)	ρ_{calc}(g/cm^3)	N_{meas}/N_{uniq}	R_I
15	10.4293(10)	1134.4(3)	4.462(1)	2958/861	0.0425
100	10.4311(10)	1134.9(3)	4.460(1)	2933/855	0.0520
150	10.4285(10)	1134.1(3)	4.463(1)	2822/843	0.0545
200	10.4289(11)	1134.2(4)	4.463(1)	2745/829	0.0531
300	10.4432(9)	1138.9(3)	4.444(1)	3692/868	0.0668
450	10.5028(11)	1158.6(4)	4.369(1)	1686/617	0.0731
600	10.5115(14)	1161.4(5)	4.358(2)	1274/537	0.0603
900	10.5541(16)	1175.6(5)	4.306(2)	818/337	0.0808

were corrected for the Lorentz factor and normalized based on the measured spectral distribution of the incident beam and detector efficiency. The data were also corrected for absorption using the measured crystal morphology [μ_a(true absorption at 1.8 Å) = 0.0509 cm^{-1}, μ_s(total scattering) = 0.1768 cm^{-1}]. Neutron absorption cross sections were taken from Sears.[30] Further experimental details are listed in Table I.

B. Powder synchrotron x-ray diffraction

High-resolution synchrotron powder diffraction measurements were carried out at the beam line BL02B2 at SPring8, Japan. A large Debye-Scherrer camera with an image plate detector was used to record the data.[31] The samples were sealed in 0.1 mm glass capillaries, which were mounted in a helium Displex refrigerator and the temperature was controlled to within 1 K. For the $Ba_8In_{16}Ge_{30}$ sample, the temperature control was obtained with a nitrogen gas flow system. The incident x-ray wavelength ($\lambda = 0.44998$ Å) was determined by calibration on a standard CeO_2 sample ($a = 5.411102$ Å). The use of high energy radiation in combination with minute samples effectively reduces systematic errors such as extinction, absorption, and anomalous scattering. The image plates were scanned with a pixel resolution of 100 μm. Data sets were recorded between 15 and 300 K. Rietveld refinements were performed using GSAS.[32] The backgrounds were described by an interpolation formula linear in 2θ (36 parameters), and the peak profiles by a pseudo-Voigt function (three parameters). All data sets extend from $2\theta = 3°$ to $2\theta = 75°$ with a step size of 0.01°, although for $Ba_8In_{16}Ge_{30}$ the high order reflections were weak, and only data with $2\theta < 44°$ were used in the refinements. The displex refrigerator induces jumps in the background and the regions 47°–52° and 59°–61° were excluded from the fit. Figures 2(a)–2(d) show the observed and modeled diffraction diagrams for the four different structures at 300 K. Crystallographic details and refined structural parameters are given in Tables. II–V.

C. Synthesis

All compounds were synthesized according to previously reported methods in Ref. 7, although the $Sr_8Ga_{16}Ge_{30}$ and $Ba_8Ga_{16}Ge_{30}$ samples are not from the same batch as the samples studied in Ref. 7. All samples are *n*-type. A study of the crystallographic differences between *n*- and *p*-type $Ba_8Ga_{16}Ge_{30}$ is in preparation.[33]

III. $Ba_8Ga_{16}Si_{30}$ SINGLE CRYSTAL NEUTRON DATA

The clathrate type I structure consists of a cubic lattice of pentagonal dodecahedra (20 atom), Fig. 1. The internal voids of the structure are tetrakaidecahedra (24 atoms) cages joined at the hexagonal faces. Each unit cell contains two small dodecahedra and six large tetrakaidecahedra. For the four materials studied here the polyhedra are formed by tetrahedrally bonded Ga, In, Si, or Ge atoms. The guest atoms (Ba and Sr) in the small cages we denote M1 (2*a* site), and the guest atoms in the large cages M2 (6*d* site). The M2 atoms form a linear chain through the structure "broken" by the hexagonal windows of the framework. A framework that consists of one type of atoms only, or a framework that consists of several types of completely random positioned atoms, will have $Pm\bar{3}n$ symmetry with three different framework sites with Wyckoff notation 6*c*, 16*i*, and 24*k*, and atoms on these sites are referred to as H_{6c}, H_{16i}, and H_{24k}, respectively.

Initial refinements of the multiwavelength time-of-flight neutron data were carried out with the program GSAS.[32] Each framework site was constrained to be fully occupied but the relative Ga/Si content was allowed to vary unconstrained. The positions and the temperature factors of the Ga and Si atoms were kept identical. Since the 300 K data set is the largest, this was used for deducing the Ga/Si occupation, which refined to 0.626(9)/0.374(9), 0.111(6)/0.889(6), and 0.425(7)/0.575(7) for the 6*c*, 16*i*, and 24*k* site, respectively. The Ga atoms prefer the six-ring environment of the 6*c* sites, whereas the Si atoms prefer the perfect tetrahedral arrangement of the 16*i* site. The refined occupation corresponds to a stoichiometry of $Ba_8Ga_{15.7(2)}Si_{30.3(2)}$ suggesting an *n*-type sample.[10,26,34,35] Refinements at the other temperatures give identical results within the estimated standard uncertainties.

Based on the initial structural refinements the data were corrected for extinction and equivalent reflections were averaged with program SORTAV,[36] see Table I. For later use, the unit cell expansion was parameterized as seen from the upper

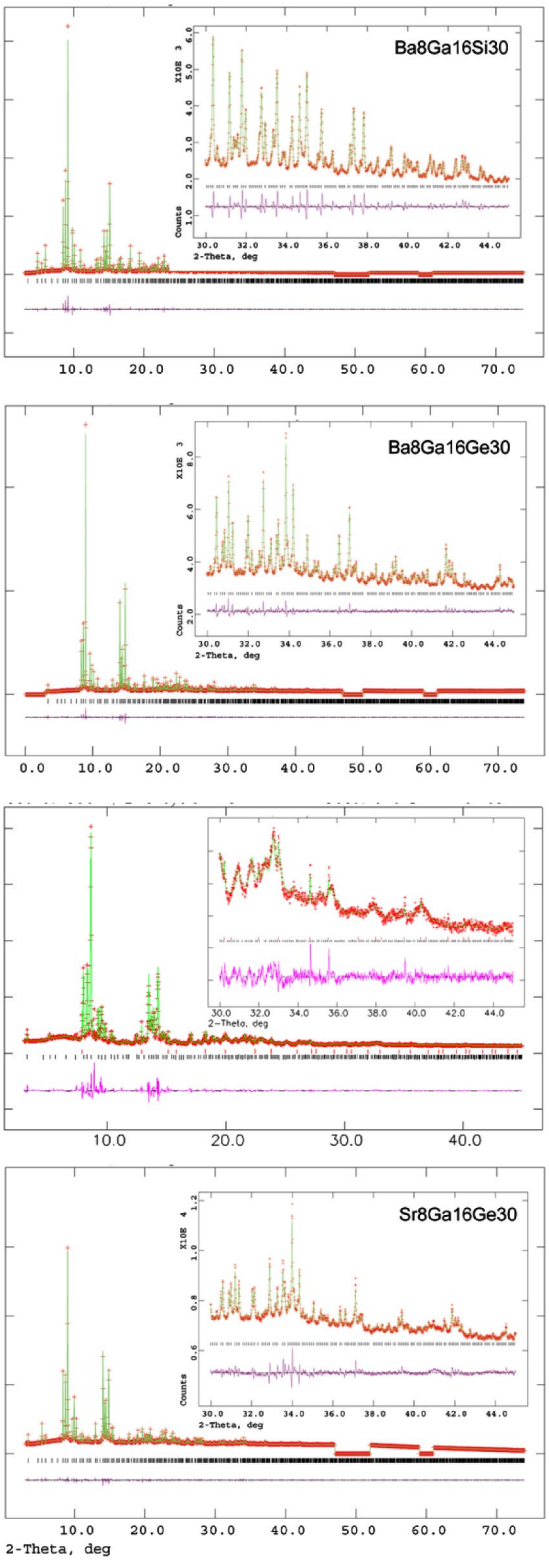

FIG. 2. (Color online) Observed and calculated diffraction patterns at 300 K as a function of 2θ for $Ba_8Ga_{16}Si_{30}$, $Ba_8Ga_{16}Ge_{30}$, $Ba_8In_{16}Ge_{30}$, and $Sr_8Ga_{16}Ge_{30}$. Curves below the diffraction patterns are the observed intensities minus the model intensities. The insets show that detailed features are also observed at higher 2θ angles.

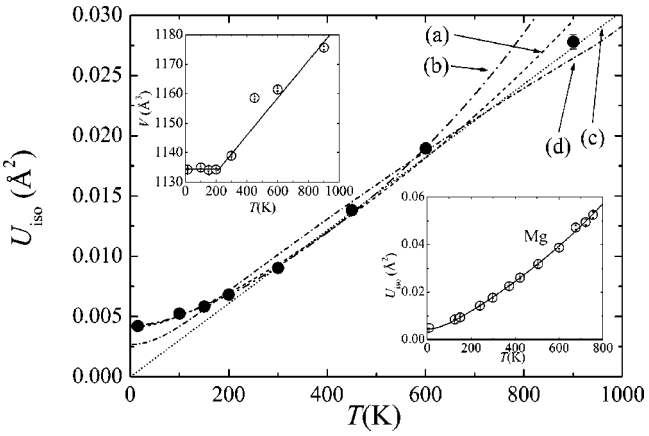

FIG. 3. Isotropic mass and site averaged framework atomic displacement parameters (U_{iso}) as a function of temperature (T) for $Ba_8Ga_{16}Si_{30}$ obtained from single crystal neutron diffraction. Curve (a) is a fit to a Debye model with $\theta_D=387(11)$ K, $d=0.043(3)$ Å, $\gamma_G=3.5(10)$. Curve (b) is a fit to the same model but with the 900 K data point excluded [$\theta_D=403(7)$ K, $d=0.046(1)$ Å, $\gamma_G=6.1(8)$]. Line (c) is a high temperature approximation of the Debye model with $\theta_D=336(3)$. It is seen that line (c) crosses approximately (0,0) as expected if no disorder and zero-point vibration is present. Curve (d) shows that a fit to all data points with $d=0$ is poor [$\theta_D=321(11)$ K, $\gamma_G=-1.7(27)$]. The lower right inset shows U_{iso} for Mg as a function of temperature (Ref. 39). The solid curve is fit to a Debye model without disorder [$\theta_D=333(3)$ K and $\gamma_G=2.2(2)$]. The upper left inset shows the volume (V) of the unit cell of $Ba_8Ga_{16}Si_{30}$ as a function of temperature. The solid lines are a parameterization used for modeling $U_{iso}(T)$, see text.

left inset in Fig. 3. Already at this point it may be noted that the 450 K data point appears to be an outlier. We have extensively analyzed the structure factor residuals after refinement of the 450 K data, but we have not been able to find systematic trends like particularly large errors in the high order data, or in the strong data or in certain regions of reciprocal space. Subsequent structure factor fitting was carried out with the program XD.[37] As mentioned in the Introduction several models describing the disorder of the guest atom in the large cage of $Sr_8Ga_{16}Ge_{30}$ fit the data equally well.[21–23] In the present case the equivalent split site model for Ba2 diverges for all data sets, because the positional parameter correlates with the anisotropic ADPs. Therefore a split site model with Ba2 on the 24*j* site and isotropic ADPs was used. Using the 24*j* site to describe the disorder only introduces one independent positional parameter, whereas the 24*k* site involves two independent positional parameters and refinements become less stable. Finally, also the anharmonic model of Ref. 23 was employed. Ga and Si atoms on identical sites were constrained to have the same positional and thermal parameters, and in Table VI the refinement residuals for the different structural models are listed. The split site model and the anharmonic model do not improve the residuals or χ^2 significantly. Tables VII and VIII contain selected structural parameters of the three models. For the framework atoms there is no systematic change in the positions of the atoms with temperature. In the isotropic split-model Ba2 tends to move away from the center of the cage

TABLE II. Crystallographic details and refined parameters from Rietveld analysis of synchrotron powder diffraction data on $Ba_8Ga_{16}Si_{30}$. The guest atom in the small cavity, M1, is at (0, 0, 0), and in the large cavity, M2, at (1/4, 1/2, 0). One framework atom, H_{6c} is located on the (1/4, 0, 1/2) 6*c* special position.

T (K)	20	35	50	65	80	95	110	125
Exposure time (min)	30	30	30	30	30	30	30	30
No. of data points	6358	6359	6358	6358	6358	6358	6369	6360
No. of reflections	2244	2244	2244	2244	2250	2250	2250	2250
No. of parameters	55	55	55	55	55	55	55	55
R_p (%)	3.05	3.23	2.91	3.03	3.13	2.97	2.97	2.96
R_{wp} (%)	4.62	4.98	4.35	4.60	4.83	4.51	4.46	4.55
χ^2 (%)	6.68	7.76	5.71	6.55	7.17	6.22	5.99	6.17
R_I (%)	5.42	5.55	5.36	5.42	5.43	5.37	5.51	5.57
a(Å)	10.5004(1)	10.5017(1)	10.5019(1)	10.5033(1)	10.5047(1)	10.5058(1)	10.5068(1)	10.5080(1)
$U_{11}=U_{22}=U_{33}$ (M1) (10^{-5} Å^2)	349(19)	399(21)	455(19)	454(20)	498(22)	515(21)	540(21)	596(22)
U_{11} (M2) (10^{-5} Å^2)	439(39)	531(44)	580(38)	577(41)	616(45)	713(43)	729(43)	801(44)
$U_{22}=U_{33}$ (M2) (10^{-5} Å^2)	1638(29)	1720(32)	1776(28)	1884(31)	1912(33)	2003(32)	2131(32)	2246(33)
Occupancy Si (H_{6c})	0.388(2)	0.398(2)	0.393(2)	0.391(2)	0.385(2)	0.394(2)	0.395(2)	0.396(2)
Occupancy Si (H_{16i})	0.916(2)	0.917(2)	0.919(2)	0.915(2)	0.917(2)	0.920(2)	0.918(2)	0.918(2)
Occupancy Si (H_{24k})	0.601(2)	0.592(2)	0.595(2)	0.595(2)	0.596(2)	0.598(2)	0.597(2)	0.597(2)
$x=y=z$ (H_{16i})	0.1852(1)	0.1855(1)	0.1855(1)	0.1854(1)	0.1855(1)	0.1854(1)	0.1853(1)	0.1853(1)
y (H_{24k})	0.3063(1)	0.3062(1)	0.3062(1)	0.3063(1)	0.3062(1)	0.3061(1)	0.3061(1)	0.3062(1)
z (H_{24k})	0.1187(1)	0.1192(1)	0.1192(1)	0.1192(1)	0.1191(1)	0.1193(1)	0.1193(1)	0.1194(1)
U_{iso} (Frame) (10^{-5} Å^2)	407(18)	409(20)	421(17)	430(18)	452(20)	467(19)	496(19)	538(19)
T (K)	150	175	200	225	250	275	300	
Exposure time (min)	30	30	30	30	30	30	30	
No. of data points	6358	6358	6359	6358	6358	6359	6359	
No. of reflections	2253	2253	2253	2256	2256	2256	2256	
No. of parameters	55	55	55	55	55	55	55	
R_p (%)	2.97	3.01	2.89	2.90	2.93	3.08	3.04	
R_{wp} (%)	4.56	4.63	4.53	4.51	4.54	4.60	4.61	
χ^2 (%)	6.23	6.49	6.27	6.24	6.42	6.74	7.17	
R_I (%)	5.47	5.48	5.39	5.32	5.39	5.68	5.88	
a(Å)	10.5107(1)	10.5132(1)	10.5154(1)	10.5176(1)	10.5201(1)	10.5263(1)	10.5271(1)	
$U_{11}=U_{22}=U_{33}$ (M1) (10^{-5} Å^2)	634(23)	691(24)	739(24)	777(25)	831(26)	875(27)	911(25)	
U_{11} (M2) (10^{-5} Å^2)	875(46)	944(49)	1061(50)	1097(50)	1187(52)	1303(55)	1375(55)	
$U_{22}=U_{33}$ (M2) (10^{-5} Å^2)	2380(35)	2496(37)	2631(38)	2765(38)	2933(40)	3056(55)	3188(41)	
Occupancy Si (H_{6c})	0.387(2)	0.387(2)	0.387(2)	0.390(2)	0.384(2)	0.394(2)	0.394(2)	
Occupancy Si (H_{16i})	0.915(2)	0.919(2)	0.920(2)	0.923(2)	0.924(2)	0.927(2)	0.925(2)	
Occupancy Si (H_{24k})	0.598(2)	0.598(2)	0.599(2)	0.601(2)	0.600(2)	0.603(2)	0.601(2)	
$x=y=z$ (H_{16i})	0.1854(1)	0.1854(1)	0.1855(1)	0.1855(1)	0.1854(1)	0.1854(1)	0.1853(1)	
y (H_{24k})	0.3062(1)	0.3061(1)	0.3060(1)	0.3060(1)	0.3059(1)	0.3059(1)	0.3059(1)	
z (H_{24k})	0.1192(1)	0.1193(1)	0.1193(1)	0.1193(1)	0.1192(1)	0.1191(1)	0.1192(1)	
U_{iso} (Frame) (10^{-5} Å^2)	574(20)	608(21)	639(21)	668(21)	723(22)	761(23)	826(20)	

with increasing temperature. The physical significance of this result should be treated with some care since the positional parameter (y) may correlate with the isotropic ADPs of Ba2. However, the model free MEM nuclear densities described below support the result. Further discussion of this aspect can be found in Ref. 24. Below 300 K the thermal parameters for Ga/Si on the 16*i* site are slightly higher than the thermal parameters for the other two sites. This agrees with the refined occupation, where it was found that light mass Si dominates on this site.

In the following we analyze the temperature dependence of the ADPs of the framework atoms. We have not made a detailed analysis for each framework site but compressed the data by calculating a mass and site averaged isotropic ADP (U_{iso}). Figure 3 shows U_{iso} as a function of temperature. In the Debye model[38]

TABLE III. Crystallographic details and refined parameters from Rietveld analysis of synchrotron powder diffraction data on $Ba_8Ga_{16}Ge_{30}$. The guest atom in the small cavity, M1, is at (0, 0, 0), and in the large cavity, M2, at (1/4, 1/2, 0). One framework atom, H_{6c} is located on the (1/4, 0, 1/2) 6*c* special position.

T (K)	15	40	50	60	100	150	200	250
Exposure time (min)	50	50	50	50	50	50	50	50
No. of data points	6593	6593	6593	6593	6597	6596	6593	6593
No. of reflections	2426	2394	2394	2394	2397	2397	2402	2402
No. of parameters	49	49	49	49	49	49	49	49
R_p (%)	1.55	1.66	1.66	1.76	1.79	2.08	1.59	1.63
R_{wp} (%)	2.71	2.56	2.54	2.63	2.71	2.89	2.49	2.51
χ^2 (%)	3.71	2.99	2.62	2.63	2.63	0.62	2.61	2.69
R_I (%)	3.52	3.30	3.16	3.52	3.46	4.43	3.74	4.12
a(Å)	10.74394(5)	10.74398(5)	10.74398(5)	10.74366(6)	10.75032(6)	10.75247(6)	10.75618(5)	10.76035(6)
$U_{11}=U_{22}=U_{33}$ (M1) (10^{-5} Å^2)	449(21)	518(20)	526(20)	571(22)	614(23)	691(25)	816(22)	937(24)
U_{11} (M2) (10^{-4} Å^2)	846(42)	883(39)	920(40)	903(42)	1045(46)	997(49)	1410(45)	1547(48)
$U_{22}=U_{33}$ (M2) (10^{-5} Å^2)	2747(33)	2828(31)	2860(32)	2923(34)	3151(37)	3319(40)	3820(36)	4192(39)
$x=y=z$ (H_{16i})	0.18456(3)	0.18457(3)	0.18458(3)	0.18465(3)	0.18462(3)	0.18473(4)	0.18461(3)	0.18464(3)
y (H_{24k})	0.30859(5)	0.30857(5)	0.30859(5)	0.30852(5)	0.30850(5)	0.30838(6)	0.30851(5)	0.30845(5)
z (H_{24k})	0.11803(5)	0.11799(5)	0.11806(5)	0.11808(5)	0.11821(5)	0.11785(6)	0.11816(5)	0.11818(5)
U_{iso} (Frame) (10^{-5} Å^2)	453(8)	498(8)	513(8)	535(9)	597(9)	616(10)	759(9)	873(10)
T (K)	300							
Exposure time (min)	50							
No. of data points	6593							
No. of reflections	2414							
No. of parameters	49							
R_p (%)	1.65							
R_{wp} (%)	2.55							
χ^2 (%)	2.96							
R_I (%)	3.51							
a(Å)	10.76388(5)							
$U_{11}=U_{22}=U_{33}$ (M1) (10^{-5} Å^2)	1053(23)							
U_{11} (M2) (10^{-5} Å^2)	1752(51)							
$U_{22}=U_{33}$ (M2) (10^{-5} Å^2)	4482(41)							
$x=y=z$ (H_{16i})	0.18458(4)							
y (H_{24k})	0.30845(5)							
z (H_{24k})	0.11821(5)							
U_{iso} (Frame) (10^{-5} Å^2)	957(10)							

$$U_{iso} = \frac{3\hbar^2 T}{m k_B \theta_D^2}\left[\frac{T}{\theta_D}\int_0^{\theta_D/T}\frac{x}{e^x-1}dx + \frac{\theta_D}{4T}\right] + d^2, \qquad (1)$$

where T is the temperature, m is the average mass, θ_D is the Debye temperature, and d is an empirical term describing temperature independent disorder. The Debye model assumes that the unit cell has a fixed volume as a function of temperature. By introducing the Grüneisen parameter (γ_G) one can circumvent this and make the expression volume dependent. From the definition of γ_G, $\Delta\omega(T)/\omega(T_0) = -\gamma_G \Delta V(T)/V(T_0)$,[38] it is seen that θ_D can be rewritten as $\theta_D(T_0)\{1-\gamma_G[V(T)-V(T_0)]/V(T_0)\}$. In the following $T_0 = 0$ K is used. Using the experimentally determined lattice constants (upper inset in Fig. 3) and fitting the above equation by numerical methods we obtain $\theta_D(T_0) = 387(11)$K, $\gamma_G = 3.5(10)$, and $d = 0.044(2)$ Å [curve (a) in Fig. 3]. The 900 K data point is slightly lower than predicted by the model. This can be due to *thermal diffuse scattering* (TDS) which can give significant contributions to the Bragg peaks at high temperatures. TDS increases with scattering angle and to a first approximation it correlates 100% with the thermal parameters.[38] The effect of noncorrected TDS is thus to make the ADPs smaller. We have repeated the fitting with the 900 K data point excluded, but with respect to θ_D and d this gives essentially the same result [curve (b), $\theta_D = 403(7)$ K, $\gamma_G = 6.1(8)$, $d = 0.046(1)$ Å]. If the data points at and above 300 K are fitted to a model with γ_G constrained to zero one obtains $\theta_D = 336$ K and $d \approx 0$. The dotted straight line (c) is the high temperature approximation of the Debye model with

TABLE IV. Crystallographic details and refined parameters from Rietveld analysis of synchrotron powder diffraction data on $Ba_8In_{16}Ge_{30}$. The guest atom in the small cavity, M1, is at (0, 0, 0), and in the large cavity, M2, at (1/4, 1/2, 0). One framework atom, H_{6c} is located on the (1/4, 0, 1/2) 6*c* special position.

T (K)	105	120	135	165	180	195	225	240
Exposure time (min)	10	10	10	10	10	10	10	10
No. of data points	4099	4099	4099	4099	4099	4099	4099	4099
No. of reflections	748	748	748	748	748	748	750	750
No. of parameters	54	54	54	54	54	54	54	54
R_p (%)	4.76	5.63	5.38	4.66	4.66	4.58	4.53	4.49
R_{wp} (%)	7.79	9.22	8.95	7.73	7.72	7.57	7.60	7.56
χ^2 (%)	6.38	9.07	8.38	6.16	6.07	5.90	5.93	5.92
R_I (%)	4.91	5.89	6.09	5.11	5.16	5.14	5.22	5.44
a(Å)	11.0984(6)	11.0996(6)	11.1017(6)	11.1061(6)	11.1081(6)	11.1101(6)	11.1154(6)	11.1175(7)
$U_{11}=U_{22}=U_{33}$ (M1) (10^{-4} Å^2)	71(20)	74(21)	79(21)	96(21)	106(22)	114(22)	129(23)	127(23)
U_{11} (M2) (10^{-4} Å^2)	145(8)	148(42)	161(42)	181(43)	193(44)	223(46)	250(48)	257(48)
$U_{22}=U_{33}$ (M2) (10^{-4} Å^2)	831(39)	850(40)	868(41)	895(41)	902(42)	909(42)	953(44)	957(44)
Occupancy In (H_{6c})	0.472(38)	0.464(39)	0.489(39)	0.481(39)	0.488(39)	0.495(39)	0.498(39)	0.501(39)
Occupancy In (H_{16i})	0.803(40)	0.790(40)	0.804(40)	0.813(39)	0.829(40)	0.815(40)	0.827(41)	0.825(41)
Occupancy In (H_{24k})	0.761(34)	0.755(34)	0.769(34)	0.778(34)	0.795(34)	0.789(35)	0.801(35)	0.798(35)
$x=y=z$ (H_{16i})	0.1844(2)	0.1843(2)	0.1844(2)	0.1844(2)	0.1844(2)	0.1844(2)	0.1843(2)	0.1843(2)
y (H_{24k})	0.3049(3)	0.3050(3)	0.3048(3)	0.3049(3)	0.3049(3)	0.3048(3)	0.3048(3)	0.3048(3)
z (H_{24k})	0.1166(3)	0.1167(3)	0.1165(3)	0.1165(3)	0.1166(3)	0.1166(3)	0.1165(3)	0.1166(3)
U_{iso} (Frame) (10^{-5} Å^2)	1451(83)	1455(84)	1515(85)	1690(87)	1685(88)	1755(90)	1882(92)	1938(94)
T (K)	255	285	300					
Exposure time (min)	10	10	10					
No. of data points	4099	4099	4099					
No. of reflections	750	738	740					
No. of parameters	54	54	54					
R_p (%)	4.40	4.32	4.21					
R_{wp} (%)	7.43	7.41	7.18					
χ^2 (%)	5.77	6.24	7.99					
R_I (%)	4.41	5.18	4.30					
a(Å)	11.1195(7)	11.1242(6)	11.1455(10)					
$U_{11}=U_{22}=U_{33}$ (M1) (10^{-4} Å^2)	138(23)	157(24)	174(37)					
U_{11} (M2) (10^{-4} Å^2)	266(49)	285(49)	425(72)					
$U_{22}=U_{33}$ (M2) (10^{-4} Å^2)	962(44)	1014(45)	940(71)					
Occupancy In (H_{6c})	0.512(40)	0.517(40)	0.487(85)					
Occupancy In (H_{16i})	0.824(41)	0.828(41)	0.826(72)					
Occupancy In (H_{24k})	0.804(35)	0.817(35)	0.787(69)					
$x=y=z$ (H_{16i})	0.1843(2)	0.1844(2)	0.1840(3)					
y (H_{24k})	0.3049(3)	0.3047(3)	0.3046(5)					
z (H_{24k})	0.1166(3)	0.1166(3)	0.1170(4)					
U_{iso} (Frame) (10^{-5} Å^2)	1986(94)	2086(95)	2306(144)					

$\theta_D(T_0)=336$ K and $d=0$. Line (c) shows that disorder does not need to be introduced to model the high temperature data well. However, if the d^2 term is excluded when modeling all the data, the fit deteriorates significantly. This is line (d) of Fig. 3, where d has been constrained to zero [$\theta_D=321(11)$ K, $\gamma_G=-1.7(27)$]. For comparison U_{iso} for metallic magnesium, based on literature data,[39] has been inserted in Fig. 3. The solid line in the inset is a fit with $\theta_D=333(3)$ K, $\gamma G=2.2(2)$ and d constrained to zero. A literature value for θ_D is 340 K,[40] indeed in good agreement.

It is obvious from the above analysis that within the Debye model the low and high temperature ADPs are not in accordance with each other. Although it can be interpreted as if the phonon dispersion relation may not be of Debye type we believe that it is a consequence of positional disorder on the framework sites. The distribution of Ga and Si on the

TABLE V. Crystallographic details and refined parameters from Rietveld analysis of synchrotron powder diffraction data on $Sr_8Ga_{16}Ge_{30}$. The guest atom in the small cavity, M1, is at (0, 0, 0), and in the large cavity, M2, at (1/4, 1/2, 0). One framework atom, H_{6c} is located on the (1/4, 0, 1/2) 6*c* special position.

T (K)	20	50	110	160	210	260	300
Exposure time (min)	90	80	80	80	80	80	80
No. of data points	6396	6396	6396	6396	6396	6396	6396
No. of reflections	2369	2369	2371	2371	2379	2386	2386
No. of parameters	49	49	49	49	49	49	49
R_p (%)	1.32	1.30	1.28	1.25	1.22	1.23	1.26
R_{wp} (%)	1.99	1.94	1.91	1.88	1.88	1.88	1.98
χ^2 (%)	3.21	2.83	2.44	2.32	2.36	2.40	2.93
R_I (%)	8.71	9.05	9.28	9.21	8.75	9.37	8.61
a(Å)	10.6926(1)	10.6965(1)	10.7016(1)	10.7083(1)	10.7155(1)	10.7219(1)	10.7274(1)
$U_{11}=U_{22}=U_{33}$ (M1) (10^{-4} Å^2)	94(5)	97(5)	104(5)	113(5)	133(5)	139(5)	149(5)
U_{11} (M2) (10^{-4} Å^2)	198(11)	201(11)	214(11)	249(12)	255(12)	292(13)	339(14)
$U_{22}=U_{33}$ (M2) (10^{-4} Å^2)	1382(13)	1370(13)	1370(13)	1373(13)	1399(13)	1413(13)	1420(14)
$x=y=z$ (H_{16i})	0.18395(4)	0.18401(4)	0.18403(4)	0.18398(4)	0.18400(5)	0.18397(5)	0.18386(5)
y (H_{24k})	0.30963(6)	0.30961(6)	0.30958(6)	0.30961(6)	0.30957(6)	0.30953(6)	0.30953(7)
z (H_{24k})	0.11736(6)	0.11742(6)	0.11742(6)	0.11762(6)	0.11761(6)	0.11768(6)	0.11770(6)
U_{iso} (Frame) (10^{-5} Å^2)	857(12)	871(12)	930(13)	1036(13)	1147(14)	1237(15)	1324(18)

three framework sites is almost random even though they have preferred sites. From this it follows that each framework site has an almost random distribution of Ga/Si as nearest neighbors. This leads to small differences in the bond lengths and the framework atoms therefore have a distribution of positions around their respective crystallographic sites. We therefore believe that *d* is a measure of the average displacement away from the positions obtained from modeling of the diffraction data. This is also supported by the fact that the differences in covalent bond lengths between Ga—Ga, Si—Si, and Ga—Si bonds are of the same magnitude as *d*.

IV. SYNCHROTRON POWDER DIFFRACTION DATA

For each sample and temperature the diffraction pattern has been modeled with an ordered, harmonic model with isotropic ADPs, except for M2 where anisotropic ADPs were used. The ADPs for all framework sites are constrained to be the same. For $Ba_8Ga_{16}Si_{30}$ and $Ba_8In_{16}Ge_{30}$ the distribution of Ga/In and Si/Ge, respectively, on the three framework sites was also refined. For $Ba_8Ga_{16}Ge_{30}$ and $Sr_8Ga_{16}Ge_{30}$ this is not possible since the x-ray contrast between Ga and Ge is too small. The $Ba_8In_{16}Ge_{30}$ powder sample contained two foreign phases. One could be identified as Ge, which was included in the modeling. This adds three more parameters to the model (unit cell parameter, ADP, and relative amount). The Ge content was refined to approximately 2.5% (atomic). The second phase could not be identified but comparing the intensities of the unique peaks with the intensities of the main phase peaks we estimate the amount to be low [probably less than 1% (atomic)]. Inclusion of the Ge impurity in the Rietweld refinement changes the fitted parameters for $Ba_8In_{16}Ge_{30}$ insignificantly. The same is very likely to be the case for the unidentified phase. Figure 2 contains the diffraction patterns at 300 K and the corresponding model patterns for each sample. It is seen that the residuals of the modeling are slightly larger for $Ba_8In_{16}Ge_{30}$. This is probably due to the unidentified phase and shorter measurement time. Tables II–V summarize some of the experimental details and parameters obtained from the modeling. Table IX contains bond lengths and angles. For both $Ba_8Ga_{16}Si_{30}$ and $Ba_8In_{16}Ge_{30}$ the refined framework atom distribution is almost independent of temperature with a variation of less than three standard deviations. For $Ba_8Ga_{16}Si_{30}$ the average Si occupation is 0.390, 0.920, and 0.598 on the 6*c*, 16*i*, and 24*k* site, respectively, and this corresponds to a refined stoichiometry $Ba_8Ga_{14.6}Si_{31.4}$. These results are within 5% of the values obtained from the neutron diffraction experiments and similar to other literature values.[11,16] For $Ba_8In_{16}Ge_{30}$ the corresponding occupations of Ge are 0.493, 0.815, and 0.790 on the 6*c*, 16*i*, and 24*k* site, respectively, which are similar to previously reported conventional x-ray powder diffraction values.[11] The refined occupancies correspond to $Ba_8In_{11.1}Ge_{34.9}$. In Ref. 17 it is proposed that vacancies appear in $Ba_8In_{16}Ge_{30}$ when the composition is off-stoichiometric ($Ba_8In_xGe_{42-3/4x}\square_{4-1/4x}$, where $\square$ represents a vacancy) to balance the electron count. Comparison of our lattice parameter at 300 K with Ref. 17 suggests that the stoichiometry is $Ba_8In_{13}Ge_{32.25}\square_{0.75}$. We are, however, not able to refine the presence of vacancies because this leads to a large correlation between the thermal and occupational parameters. Instead, we have tested models where a fixed number of vacancies (N_v) were introduced. This changes the framework ADPs of the order $N_v/46$ and this is less than 4% for any realistic amount of vacancies.

In $Ba_8Al_{16}Ge_{30}$ the 6*c* and 24*k* sites are occupied completely by Al and Ge, respectively, whereas the 16*i* site is

TABLE VI. Refinement residuals for the single crystal neutron data. In model 1 the guest atoms are located at the centers of the cages, whereas in model 2 the Ba(2) atoms are disordered at site 24*j*. Model 1 employs anisotropic harmonic ADPs on all atoms, whereas in model 2 Ba(2) is isotropic. In model 3 anharmonic Gram-Charlier expansions to fourth order are included on the guest atoms. The first line lists $R(F)$, second line $R_w(F)$, third line $R(F^2)$, fourth line $R_w(F^2)$, and fifth line goodness of fit.

T (K)		Model 1	Model 2	Model 3	MEM
15	$R(F)$	0.0460	0.0459	0.0464	0.0468
	$R_w(F)$	0.0272	0.0270	0.0268	0.0269
	$R(F^2)$	0.0648	0.0647	0.0652	
	$R_w(F^2)$	0.0534	0.0531	0.0534	
	Goof	1.061	1.0539	1.049	
100	$R(F)$	0.0532	0.0530	0.0523	0.0522
	$R_w(F)$	0.0267	0.0265	0.0264	0.0261
	$R(F^2)$	0.0732	0.0725	0.0716	
	$R_w(F^2)$	0.0519	0.0516	0.0513	
	Goof	1.077	1.0711	1.070	
150	$R(F)$	0.0520	0.0522	0.0515	0.0517
	$R_w(F)$	0.0263	0.0261	0.0257	0.0259
	$R(F^2)$	0.0707	0.0706	0.0698	
	$R_w(F^2)$	0.0513	0.0510	0.0503	
	Goof	1.058	1.0510	1.041	
200	$R(F)$	0.0526	0.0525	0.0528	0.0539
	$R_w(F)$	0.0276	0.0271	0.0269	0.0271
	$R(F^2)$	0.0712	0.0699	0.0706	
	$R_w(F^2)$	0.0536	0.0529	0.0523	
	Goof	1.031	1.0162	1.009	
300	$R(F)$	0.0547	0.0554	0.0546	0.0568
	$R_w(F)$	0.0300	0.0302	0.0299	0.0296
	$R(F^2)$	0.0712	0.0726	0.0712	
	$R_w(F^2)$	0.0588	0.0590	0.0585	
	Goof	1.305	1.3105	1.303	
450	$R(F)$	0.0752	0.0741	0.0742	0.0705
	$R_w(F)$	0.0365	0.0363	0.0360	0.0350
	$R(F^2)$	0.1040	0.1024	0.1024	
	$R_w(F^2)$	0.0697	0.0693	0.0688	
	Goof	1.187	1.178	1.149	
600	$R(F)$	0.0728	0.0724	0.0751	0.0692
	$R_w(F)$	0.0322	0.0320	0.0311	0.0308
	$R(F^2)$	0.0944	0.0942	0.0945	
	$R_w(F^2)$	0.0627	0.0625	0.0605	
	Goof	1.149	1.1436	1.113	
900	$R(F)$	0.0806	0.0808	0.0819	0.0799
	$R_w(F)$	0.0432	0.0429	0.0426	0.0426
	$R(F^2)$	0.1180	0.1166	0.1167	
	$R_w(F^2)$	0.0847	0.0839	0.0833	
	Goof	1.717	1.6996	1.704	

shared by Al and Ge.[16] In $Ba_8Ga_{16}Ge_{30}$ and $Sr_8Ga_{16}Ge_{30}$ the x-ray contrast between Ga and Ge is small, but MEM analysis of single crystal x-ray diffraction data[7] and resonant powder diffraction measurements[41] indicate that Ga has the same site preferences as in $Ba_8Ga_{16}Si_{30}$. Although earlier measurements indicated that Ga and Ge have no preferred sites in $Sr_8Ga_{16}Ge_{30}$, $Ba_8Ga_{16}Ge_{30}$, and $Eu_8Ga_{16}Ge_{30}$.[21,22] the growing number of experiments indicate that all clathrates with a framework consisting of group III and IV elements do have preferred sites. The group III element tends to have a large

TABLE VII. Fractional coordinates for Ba(2) (1/4, y, $y+1/2$) in the 24j split-model with isotropic ADPs (model 2 in Table VI) and Ga/Si(2) (x x x) (16i) and Ga/Si(3) (0 y z) (24k) obtained from single crystal neutron data on $Ba_8Ga_{16}Si_{30}$. Ba(1) and Ga/Si(1) are located on (0 0 0) and (1/4 0 1/2), respectively. The positional parameters of the framework atoms do not change within the standard deviation between models 1, 2, and 3.

T (K)	y (Ba2)	x Ga/Si2	y Ga/Si3	z Ga/Si3
15	0.4912(2)	0.18533(3)	0.30621(4)	0.11922(4)
100	0.4899(2)	0.18542(4)	0.30615(5)	0.11917(4)
150	0.4894(2)	0.18535(4)	0.30624(5)	0.11926(5)
200	0.4884(2)	0.18539(4)	0.30610(5)	0.11925(4)
300	0.4872(3)	0.18554(4)	0.30596(6)	0.11917(5)
450	0.4861(5)	0.18554(7)	0.30590(8)	0.11964(8)
600	0.4850(5)	0.18551(6)	0.30593(8)	0.11985(8)
900	0.4799(8)	0.1855(1)	0.3066(1)	0.1192(2)

occupancy on the 6c site, and with the exception of $Ba_8Al_{16}Ge_{30}$, the group IV element prefers the 16i site, while the 24k site is more equally occupied by both groups.

The ADPs listed in Tables II–V for all measurements have been plotted in Fig. 4 as a function of temperature. The plots also include the ADPs obtained from the single crystal neutron diffraction data on $Ba_8Ga_{16}Si_{30}$. It is seen that the ADPs from the single crystal neutron data are within 5%–10% of the ADPs from the powder synchrotron data. This demonstrates that accurate positional and thermal parameters can be obtained from synchrotron powder diffraction data. This point is indeed quite far reaching. Iversen *et al.* have shown that even in the most accurate single crystal diffraction studies there are often systematic differences between the ADPs determined separately from x-ray and neutron diffraction data.[42] Only if extreme care is taken in the experimental reduction of systematic errors and in the data analysis (e.g., use of flexible aspherical electron density models) can identical parameters be obtained. It is generally assumed that powder data are less accurate than single crystal data, and for thermal parameters, especially, single crystal neutron data rank the highest. While this undoubtedly is true in many cases, it is not necessarily so for high symmetry inorganic crystal structures containing heavy elements. Such crystals often have substantial absorption and anomalous scattering effects at the wavelengths used at conventional single crystal x-ray diffractometers (Mo Kα). Furthermore, extinction effects can be severe in the low order data due to a high degree of crystal perfection. It was for these reasons we decided to collect short wavelength synchrotron powder data in thin capilaries (0.1 mm). Simulation of absorption effects in our powder data predict that they are negligible. Due to the combined use of a powder sample and short wavelength, extinction effects are also supressed and the powder furthermore takes care of potential twinning. Finally, the anomalous scattering is minimized due to the short wavelength. The fact that single crystal neutron and synchrotron powder diffraction in the present case give very similar ADPs adds confidence to the comparative analysis and physical correctness of the results.

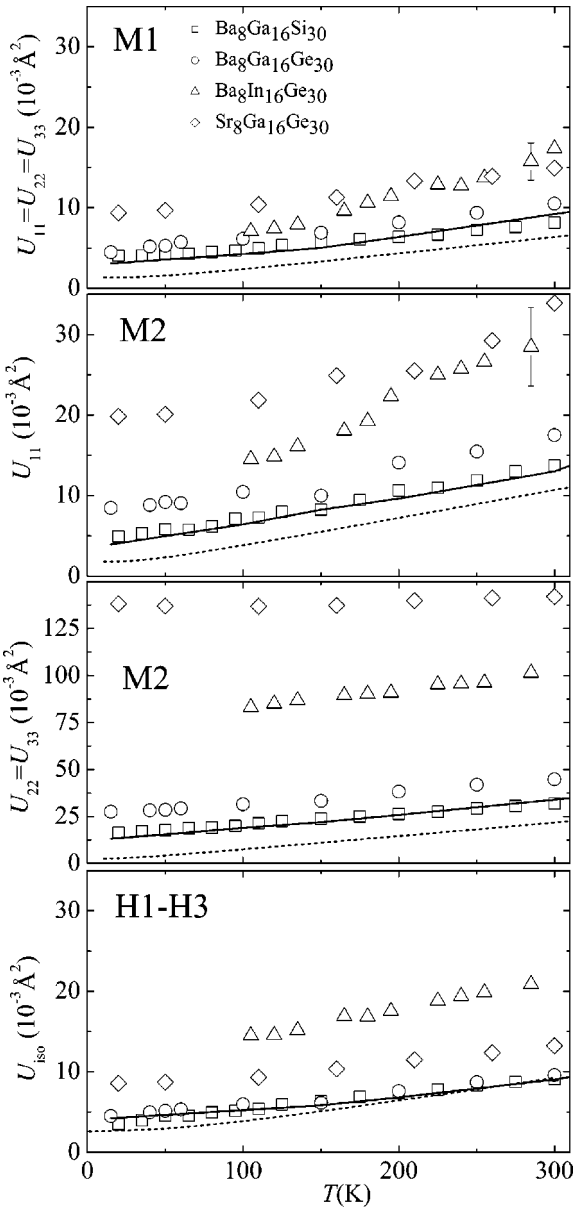

FIG. 4. Temperature (T) dependence of the framework and guest atomic displacement parameters (ADP) U. M1 are guest atoms located on the highly symmetric 2a site, M2 are guest atoms located on the 6d site. H_{6c}, H_{16i}, and H_{24k} are framework atoms on the 6c, 16i, and 24k sites. Note that the scale on the y axis is different for $U_{22}=U_{33}$ for M2. Data points are obtained from the modeling of synchrotron powder diffraction patterns. The solid curves are the corresponding data obtained from single crystal neutron diffraction on $Ba_8Ga_{16}Si_{30}$. For the upper three graphs the dotted curves are ordered Einstein models of the ADPs assuming the guest atom mass is 137.327 g/mol (Ba) and with an Einstein temperature of 130, 100, and 70 K, respectively. The dotted curve in the lower graph is an ordered Debye model of the ADPs assuming that the framework atom mass is 42.57 g/mol (weighted average of Ga and Si) and with a Debye temperature of 350 K. In all dotted curves $d=0$ has been used. The error bars are of the same size as the data points except for $U_{11}=U_{22}=U_{33}$ (2a site) and U_{11} (6d site) for Ba in $Ba_8In_{16}Ge_{30}$ where representative error bars at 285 K have been included.

TABLE VIII. Atomic displacement parameters (ADP) obtained from refinement of single crystal neutron data with a normal anisotropic and ordered model of $Ba_8Ga_{16}Si_{30}$ (model 1 in Table VI). First line is Ba(1) (2*a*), second line is Ba(2) (6*d*), third line is Ga/Si(1) (6*c*), fourth line is Ga/Si(2) (16*i*) and fifth line is Ga/Si(3) (24*k*). The ADPs of the framework atoms do not change more than one standard deviation between models 1, 2, and 3.

T (K)		U_{11} (Å^2)	U_{22} (Å^2)	U_{33} (Å^2)	U_{12} (Å^2)	U_{13} (Å^2)	U_{23} (Å^2)
15	Ba(1)	0.0031(2)	0.0031(2)	0.0031(2)	0	0	0
	Ba(2)	0.0040(4)	0.0131(3)	0.0131(3)	0	0	0
	Ga/Si(1)	0.0044(3)	0.0036(2)	0.0036(2)	0	0	0
	Ga/Si(2)	0.0049(1)	0.0049(1)	0.0049(1)	−0.0005(1)	−0.0005(1)	−0.0005(1)
	Ga/Si(3)	0.0043(2)	0.0038(1)	0.0038(1)	0	0	0.0001(1)
100	Ba(1)	0.0043(2)	0.0043(2)	0.0043(2)	0	0	0
	Ba(2)	0.0063(5)	0.0188(4)	0.0188(4)	0	0	0
	Ga/Si(1)	0.0063(3)	0.0046(2)	0.0046(2)	0	0	0
	Ga/Si(2)	0.0058(1)	0.0058(1)	0.0058(1)	−0.0005(1)	−0.0005(1)	−0.0005(1)
	Ga/Si(3)	0.0052(2)	0.0049(2)	0.0050(1)	0	0	−0.0001(1)
150	Ba(1)	0.0050(3)	0.0050(3)	0.0050(3)	0	0	0
	Ba(2)	0.0080(5)	0.0219(4)	0.0219(4)	0	0	0
	Ga/Si(1)	0.0070(3)	0.0054(2)	0.0054(2)	0	0	−0.0006(1)
	Ga/Si(2)	0.0063(1)	0.0063(1)	0.0063(1)	−0.0006(1)	−0.0006(1)	0.0000(2)
	Ga/Si(3)	0.0059(2)	0.0049(2)	0.0059(2)	0	0	
200	Ba(1)	0.0064(3)	0.0064(3)	0.0064(3)	0	0	0
	Ba(2)	0.0096(5)	0.0258(5)	0.0258(5)	0	0	0
	Ga/Si(1)	0.0074(3)	0.0064(2)	0.0064(2)	0	0	0
	Ga/Si(2)	0.0072(1)	0.0072(1)	0.0072(1)	−0.0005(1)	−0.0005(1)	−0.0005(1)
	Ga/Si(3)	0.0071(2)	0.0062(2)	0.0066(2)	0	0	0.0001(2)
300	Ba(1)	0.0092(4)	0.0092(4)	0.0092(4)	0	0	0
	Ba(2)	0.0119(7)	0.0339(6)	0.0339(6)	0	0	0
	Ga/Si(1)	0.0095(4)	0.0087(3)	0.0087(3)	0	0	0
	Ga/Si(2)	0.0095(1)	0.0095(1)	0.0095(1)	−0.0008(2)	−0.0008(2)	−0.0008(2)
	Ga/Si(3)	0.0097(2)	0.0078(2)	0.0089(2)	0	0	−0.0004(2)
450	Ba(1)	0.0133(6)	0.0133(6)	0.0133(6)	0	0	0
	Ba(2)	0.0239(13)	0.0467(10)	0.0467(10)	0	0	0
	Ga/Si(1)	0.0142(7)	0.0136(5)	0.0136(5)	0	0	0
	Ga/Si(2)	0.0141(2)	0.0141(2)	0.0141(2)	−0.0011(3)	−0.0011(3)	−0.0011(3)
	Ga/Si(3)	0.0149(4)	0.0125(4)	0.0138(4)	0	0	−0.0002(3)
600	Ba(1)	0.0182(7)	0.0182(7)	0.0182(7)	0	0	0
	Ba(2)	0.0289(14)	0.0566(11)	0.0566(11)	0	0	0
	Ga/Si(1)	0.0218(9)	0.0185(5)	0.0185(5)	0	0	0
	Ga/Si(2)	0.0187(2)	0.0187(2)	0.0187(2)	−0.0024(3)	−0.0024(3)	−0.0024(3)
	Ga/Si(3)	0.0203(4)	0.0179(4)	0.0184(3)		0	−0.0013(3)
900	Ba(1)	0.0295(15)	0.0295(15)	0.0295(15)	0	0	0
	Ba(2)	0.0400(33)	0.0883(26)	0.0883(26)	0	0	0
	Ga/Si(1)	0.0309(20)	0.0273(12)	0.0273(12)	0	0	0
	Ga/Si(2)	0.0240(5)	0.0240(5)	0.0240(5)	−0.0041(5)	−0.0041(5)	−0.0041(5)
	Ga/Si(3)	0.0314(12)	0.0248(12)	0.0320(8)	0	0	−0.0036(8)

In the following we analyze the temperature dependence of the ADPs of the guest and framework atoms in the same manner as the ADPs obtained from the single crystal neutron diffraction. The Debye model is used to describe the ADPs of the framework atoms and is given by Eq. (1), while we use an Einstein model to describe the thermal motion of the guest atoms.[24] The ADP in the Einstein model is[38,43]

$$U_{xx}^2 = \frac{\hbar^2}{2mk_B\theta_{E,xx}} \coth \frac{\theta_{E,xx}}{2T} + d^2 \qquad (2)$$

where θ_E is the Einstein temperature and the subscript refer to the direction or plane of the vibration. In this equation a d^2

TABLE IX. Bond lengths (in Å) and angles (in deg). M denotes the guest atoms at sites 2*a* and 6*d*, and H the framework atoms at 6*c*, 16*i*, and 24*k*.

	$Ba_8Ga_{16}Si_{30}$	$Ba_8Ga_{16}Ge_{30}$	$Ba_8In_{16}Ge_{30}$	$Sr_8Ga_{16}Ge_{30}$
$M1-H_{16i}$	3.379(2)	3.4412(7)	3.557(7)	3.4161(9)
$M1-H_{24k}$	3.457(1)	3.5556(6)	3.639(5)	3.5527(7)
$M2-H_{6c}$	3.72188(3)	3.80560(2)	3.9418(4)	3.79271(9)
$M2-H_{16i}$	3.9043(5)	3.9963(2)	4.142(2)	3.9868(3)
$M2-H_{24k}$	3.5602(7)	3.6209(4)	3.768(4)	3.6002(5)
$H_{6c}-H_{24k}$	2.463(1)	2.5027(6)	2.636(5)	2.4878(7)
$H_{16i}-H_{16i}$	2.359(3)	2.439(1)	2.541(13)	2.458(2)
$H_{16i}-H_{24k}$	2.4295(8)	2.4971(4)	2.567(4)	2.4922(5)
$H_{24k}-H_{24k}$	2.510(2)	2.545(1)	2.601(10)	2.525(1)
$H_{24k}-H_{6c}-H_{24k}$	108.20(2)	108.74(1)	108.6(1)	108.99(2)
$H_{24k}-H_{6c}-H_{24k}$	112.05(5)	111.94(3)	111.3(2)	110.43(3)
$H_{16i}-H_{16i}-H_{24k}$	109.10(4)	108.44(2)	109.2(2)	108.00(3)
$H_{24k}-H_{16i}-H_{24k}$	109.84(4)	110.49(2)	109.8(2)	110.90(2)
$H_{6c}-H_{24k}-H_{16i}$	105.87(5)	106.13(2)	105.5(2)	106.37(3)
$H_{6c}-H_{24k}-H_{24k}$	123.98(2)	124.53(1)	124.3(1)	124.78(2)
$H_{16i}-H_{24k}-H_{16i}$	106.83(6)	105.43(3)	106.2(3)	104.63(3)
$H_{16i}-H_{24k}-H_{24k}$	106.64(3)	106.62(2)	107.1(1)	106.55(2)

term has been added to describe possible temperature independent disorder.[24] Since the present data only extend up to 300 K, anharmonic effects have negligible influence on the ADPs, and the Grüneisen parameter and the temperature dependence of the unit cell volume have not been included in the model. The results of the fitting of the two models are given in Table X. Figure 4 also contains model calculations with $d=0$ in order to illustrate that $d>0$ is needed for a good description of the data. For $Ba_8Ga_{16}Si_{30}$ the neutron and synchrotron powder diffraction data essentially lead to the same results. For the Ba containing clathrates, θ_D increases from approximately 200 to 400 K with decreasing framework atom mass. The magnitude agrees well with θ_D obtained from measurements of the specific heat of $Ba_8Ga_{16}Ge_{30}$ and $Sr_8Ga_{16}Ge_{30}$ where θ_D is of the order 320–360 K.[9,26] As for the single crystal neutron data on $Ba_8Ga_{16}Si_{30}$ $d \approx 0.05-0.10$ Å is needed for a good modeling of the temperature dependence of the framework ADPs. It is interesting that d for the framework atoms in $Ba_8In_{16}Ge_{30}$ is twice as large as for the two other Ba containing clathrates. This can be explained by the larger variation between the In—In, Ge—Ge, and In—Ge bond lengths compared with the other framework types. Figure 5 shows the lattice parameters as a function of temperature. It is seen that there is a tendency for the samples with lowest θ_D to have the largest coefficient of thermal expansion ($\alpha=1/a\cdot\partial a/\partial T$). Although there exists no trivial relationship between θ_D and α this result is not surprising and adds confidence to the result that $Ba_8In_{16}Ge_{30}$ has an extraordinarily low θ_D.

θ_E for both guest atoms is also listed in Table X for all four compounds. It is somewhat surprising that all θ_E values for the Sr atoms in $Sr_8Ga_{16}Ge_{30}$ are larger than the corresponding values in any of the Ba containing clathrates. One could expect that θ_E was lower for Sr because of the larger ADPs, but theoretical values of θ_E and d from Ref. 18, obtained from density functional theory (DFT), predict the same trends. In a simple model this observation could partially be explained by the larger mass of Ba compared to Sr if it is assumed that the forces acting on the guest atoms are the same. However, the trend can be fully reproduced when the chemical bonding in clathrates is scrutinized within the quantum theory of atoms in molecules.[13] Gatti *et al.* carried out *ab initio* calculations on $Ba_8Ga_{16}Ge_{30}$ and $Sr_8Ga_{16}Ge_{30}$ to obtain the electron density of model clathrates having different Ga distributions. These electron densities were subsequently subjected to Bader topological analysis. We will not reproduce the many detailed arguments but merely note that the physical origin for the guest atom disorder is due to an energy gain when many weak guest-host bonds in a fully symmetrical clathrate cage are replaced by a few much stronger and shorter chemical bonds in the asymmetrical case. The few strong bonds have more covalent and directional character than the many weak bonds. The interesting point in the present context is that the tendency for strong directional bonding is larger for $Sr_8Ga_{16}Ge_{30}$ than for $Ba_8Ga_{16}Ge_{30}$. Thus there is a stronger guest-frame interaction in $Sr_8Ga_{16}Ge_{30}$ than in $Ba_8Ga_{16}Ge_{30}$, and this results in higher rattling frequencies. The chemical bond explanation goes even further, since it is also observed that the guest-framework bonding is stronger in the large cage of $Sr_8Ga_{16}Ge_{30}$ than in the small cage, whereas the opposite is true for $Ba_8Ga_{16}Ge_{30}$. This is also reproduced in our values of the Einstein temperatures, Table X. Thus for $Sr_8Ga_{16}Ge_{30}$ θ_E is higher for Sr2 than for Sr1, whereas for the Ba containing clathrates the opposite is observed.

Before continuing we want to make a distinction between two "types" of structural disorder for the guest atoms, even though their basic origin is the same. The first type is the

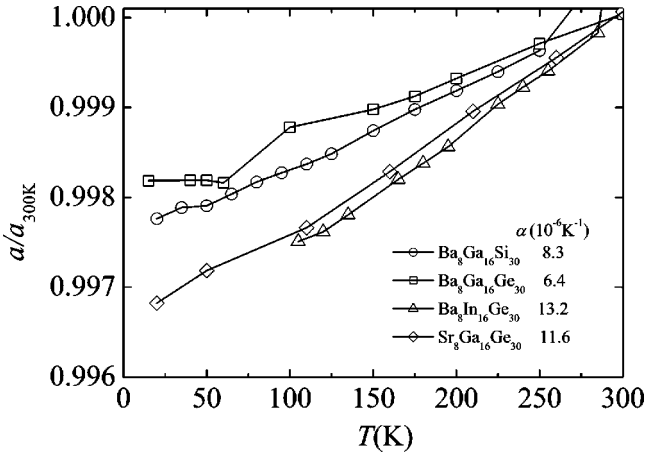

FIG. 5. Lattice parameter normalized to the 300 K value ($a/a_{300\ \mathrm{K}}$) as a function of temperature (T) for the four clathrates. Data has been calculated from Tables II–V. Since $a_{300\ \mathrm{K}}$ for $Ba_8Ga_{16}Ge_{30}$ and $Ba_8In_{16}Ge_{30}$ are slightly larger than expected and appear to be outliers, $a_{300\ \mathrm{K}}$ has been obtained by extrapolating a linear fit of $a(T)$ data above 150 K. $a_{300\ \mathrm{K},Ba_8Ga_{16}Si_{30}}=10.5303$ Å, $a_{300\ \mathrm{K},Ba_8Ga_{16}Ge_{30}}=10.7643$ Å, $a_{300\ \mathrm{K},Ba_8In_{16}Ge_{30}}=11.1649$ Å, and $a_{300\ \mathrm{K},Sr_8Ga_{16}Ge_{30}}=10.7282$ Å (compare values with $a_{300\ \mathrm{K}}$ from Tables II–V). The almost temperature independent coefficients of the thermal expansion ($\alpha=1/a\cdot\partial a/\partial T$) are listed in the inset.

case where the guest atom actually is located in the "center" of any given cage in the structure, but due to differences in the local bonding environment throughout the crystal (semirandom framework positioning) the guest atom will be slightly displaced away from the crystallographic center position from unit cell to unit cell. In the analysis of Gatti *et al.*,[13] this situation is expected for the Ba atom in the small cage of $Ba_8Ga_{16}Ge_{30}$. This type of disorder will lead to $d>0$ in the analysis of the ADPs even though the atom is located close to the center of any given cage. The second type of structural disorder is the case where it is energetically favorable for the guest atom to be displaced away from the center of the cage and form stronger directional bonds to the side of the cage, i.e., the situation for Sr in the large cage of $Sr_8Ga_{16}Ge_{30}$. This type of disorder also leads to $d>0$ and can be either static or dynamic (tunneling) depending on the shape and magnitude of the potential. A dynamic system with tunneling states requires that several potential minima for the guest atom exist within the *same* cage. When considering the asymmetric chemical interactions in any given cage, which always has a specific asymmetric distribution of Ga atoms, it seems likely that the guest atom is preferably displaced to one side of the cage. Thus a multiminima potential cannot be symmetric such as, e.g., the four-level potential used in recent tunneling models.[44] As stated in the Introduction there is no clear evidence that the disordered position is specific (24*j* or 24*k*), but rather a torus-shaped nuclear density has been observed in $Ba_8Ga_{16}Ge_{30}$, $Sr_8Ga_{16}Ge_{30}$, and $Eu_8Ga_{16}Ge_{30}$. This suggests that the observed nuclear density by crystallographic methods predominantly is a spatial average of different guest atom positions in different cages rather than a time average due to tunneling. In this picture we expect that all guest atoms in all structures are disordered. This is what is demonstrated in Table X, where $d>0$ is needed for a good modeling of the ADPs for *all* guest atoms. For the guest atoms on the 2*a* site (small cage) $d\approx0.05$ Å in the Ba containing clathrates. Since d is of the same magnitude as differences in Ba—Ge and Ba—Ga bonds this could be interpreted as being due to differences in the composition of the cages, i.e., the first type of disorder. For Sr on the 2*a* site in $Sr_8Ga_{16}Ge_{30}$ $d\approx0.09$ Å and as expected from the chemical bond analysis of Gatti *et al.* this Sr atom moves slightly off center (second type of disorder). For the guest atoms on the 6*d* site d in the [100] direction varies from about 0.05 to 0.13 Å whereas d in the (100) plane varies from about 0.1 to 0.35 Å going from $Ba_8Ga_{16}Si_{30}$ to $Sr_8Ga_{16}Ge_{30}$. In terms of the above model, this is a strong indication that the guest atoms in the large cages are displaced away from the center of the cage (second type of disorder).

V. SPECIFIC HEAT CAPACITY

From specific heat (C_p) measurements on $Ba_8Ga_{16}Ge_{30}$ θ_E has been estimated to be approximately 80 K[9,26] and 60 K.[8] This is in reasonable agreement with the results obtained from the temperature dependence of the ADPs, where averaging over all modes (Table X) gives $\theta_E=93$ K. However, for $Sr_8Ga_{16}Ge_{30}$ the agreement is less good. We obtain $\theta_E=104-163$ K from the temperature dependence of the ADPs, which is much higher than $\theta_E=55$ K[8] and 80 K[9] obtained by specific heat measurements and 46 K (32 cm^{-1}) from Raman spectroscopy.[45] Unfortunately the density of Einstein atoms is not reported in Ref. 8. In Refs. 9 and 26 the densities are approximately 16 per unit cell (u.c.) and 10 per u.c., which is larger than expected if only the guest atoms have localized vibrations. To investigate the disagreement between the values of θ_E obtained from specific heat/Raman spectroscopy and the temperature dependence of the ADPs, we have measured $C_p(T)$ of one $Ba_8Ga_{16}Ge_{30}$ sample and one $Sr_8Ga_{16}Ge_{30}$ sample, the result is shown in the inset of Fig. 6. For $Eu_8Ga_{16}Ge_{30}$ C_p is dominated by the magnetic ordering below approximately 60 K[35] and this compound is therefore not relevant for comparison. At the lowest temperatures the magnetic contribution exceeds the phononic contribution by almost one order of magnitude and heat capacity data *cannot* be used for probing the existence of tunneling states in $Eu_8Ga_{16}Ge_{30}$.[44] In the main panel we have plotted $\Delta C_p=C_{p,\mathrm{measured}}-C_{p,\mathrm{Debye}}$, where

$$C_{p,\mathrm{Debye}}(T)=9N_DR\left(\frac{T}{\theta_D}\right)^3\int_0^{\theta_D/T}\frac{x^4e^x}{(e^x-1)^2}dx \qquad (3)$$

is the specific heat from a normal Debye model. We have used $\theta_D=312$ K, obtained from the temperature dependence of the ADPs of the framework atoms (Table X), and $N_D=46$ which is the number of framework atoms. We choose to plot data in this manner because of the large normal phononic contribution to C_p which disguises information about localized vibrations. Included in the graph are also model calculations with

TABLE X. Einstein temperature (Θ_E), Debye temperature (Θ_D), and disorder parameter (d) obtained from fitting the models described in the text to the ADPs as a function of temperature. Theoretical values ($\Theta_{E,theory}, d_{theory}$) are calculated with the use of density functional theory in Ref. 18.

	Θ_E (K)	$\Theta_{E,theory}$ (K)	Θ_D (K)	d (Å)	d_{theory} (Å)
$U_{11}=U_{22}=U_{33}$ M(1)					
$Ba_8Ga_{16}Si_{30}$—neutron[a]	124	146		0.040	
$Ba_8Ga_{16}Si_{30}$—x-ray	127	146		0.052	
$Ba_8Ga_{16}Ge_{30}$	124	129		0.059	
$Ba_8In_{16}Ge_{30}$	87			0.045	
$Sr_8Ga_{16}Ge_{30}$	151	101		0.087	
U_{11} M(2)					
$Ba_8Ga_{16}Si_{30}$—Neutron[a]	98	106		0.046	
$Ba_8Ga_{16}Si_{30}$—x-ray	101	106		0.057	
$Ba_8Ga_{16}Ge_{30}$	101	79		0.081	
$Ba_8In_{16}Ge_{30}$	65			0.098	
$Sr_8Ga_{16}Ge_{30}$	104	120		0.128	
$U_{22}=U_{33}$ M(2)					
$Ba_8Ga_{16}Si_{30}$—Neutron[a]	69	59		0.103	0.13[b]
$Ba_8Ga_{16}Si_{30}$—x-ray	77	59		0.120	0.13[b]
$Ba_8Ga_{16}Ge_{30}$	73	55		0.157	0.42[b]
$Ba_8In_{16}Ge_{30}$	65			0.277	<0.60[b],[c]
$Sr_8Ga_{16}Ge_{30}$	163	107		0.368	0.81[b]
U_{iso} H_{6c}, H_{16i}, H_{24k}					
$Ba_8Ga_{16}Si_{30}$—Neutron			387	0.044	
$Ba_8Ga_{16}Si_{30}$—x-ray			416	0.045	
$Ba_8Ga_{16}Ge_{30}$			312	0.056	
$Ba_8In_{16}Ge_{30}$			203	0.098	
$Sr_8Ga_{16}Ge_{30}$			313	0.082	

[a]Results have been taken from Ref. 24.
[b]In Ref. 18 the distance from the center of the cage to the atom is calculated. This is in principle $r=\sqrt{d_{11}^2+d_{22=33}^2}$, however, r is dominated by $d_{22=33}$ since $d_{22=33}>d_{11}$ as can be seen from the table.
[c]This result is for $Ba_8In_{16}Sn_{30}$ (Ref. 18), and the result for $Ba_8In_{16}Ge_{30}$ is expected to be smaller.

$$\Delta C_p(T) = aT + \sum_i 3N_{E,i}R\left(\frac{\theta_{E,i}}{T}\right)^2 \frac{e^{\theta_{E,i}/T}}{\left(e^{\theta_{E,i}/T}-1\right)^2}, \qquad (4)$$

where the first term represents the electronic contribution linear in T and the second term is Einstein contributions from localized vibrations. For $Ba_8Ga_{16}Ge_{30}$ a relatively good agreement between ΔC_p and the model is obtained with $a=0.035$ J/(K^2 mol)/u.c. and two Einstein oscillators having $N_{E1}+N_{E2}=8$, $\theta_{E1}=80$ K ($N_{E1}=6.5$ per u.c.) and $\theta_{E2}=42$ K ($N_{E2}=1.5$ per u.c.), respectively. For $Sr_8Ga_{16}Ge_{30}$ $a=0.040$ J/(K^2 mol)/u.c., $\theta_{E1}=80$ K ($N_{E1}=6.5$ per u.c.) and $\theta_{E2}=33$ K ($N_{E2}=1.5$ per u.c.). The magnitude of a is consistent with a pure electronic contribution. If the model [Eq. (4)] only contains one Einstein oscillator a poor reproduction of the data is obtained. The wavy feature in $\Delta C_p(T)$ around 50–200 K that cannot be reproduced by our model may be due to flaws in the Debye model. This again emphasizes that the specific heat data may not give reliable information about the localized vibrations in cases where there is a large normal phononic contribution to C_p. Nevertheless, the main point is to show that the difference in $C_p(T)$ between $Ba_8Ga_{16}Ge_{30}$ and $Sr_8Ga_{16}Ge_{30}$ is relatively small.

Since N_{E1} and N_{E2} are almost 6 and 2, respectively, it would be tempting to relate the corresponding Einstein temperatures to the localized vibration of the guest atoms in the large and small cages, respectively. For $Sr_8Ga_{16}Ge_{30}$ this would also agree with the Raman spectroscopic data. Nonetheless, $\theta_{E2}=42$ K ($Ba_8Ga_{16}Ge_{30}$) and 33 K ($Sr_8Ga_{16}Ge_{30}$) are too low compared with the values obtained from the temperature dependence of the ADPs and the theoretical calculations. Instead we offer an alternative explanation for the apparent disagreement between θ_E derived from theory and the ADPs on one hand, and from $C_p(T)$ and Raman spectroscopy on the other. The theoretical value of θ_E (Ref. 18) was calculated on an energy scale of the order 0.01–1 eV (100–10 000 K). For this reason the calculation does not include nonharmonic features at the "bottom of the potential floor" that could result in a noneven separation of the lowest harmonic oscillator energy levels of say 35–45 K or lower. Considering that each cage is chemically different this suggests that the energy separation may vary from cage to cage.

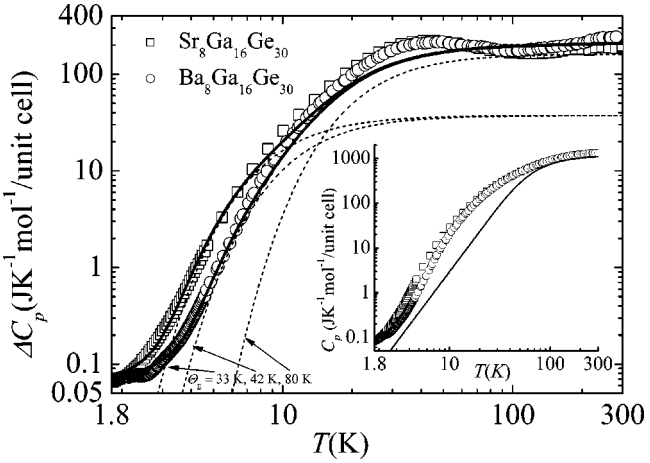

FIG. 6. The main graph shows $\Delta C_p(T) = C_{p,\mathrm{meas}} - C_{p,\mathrm{Debye}}$. The solid curves are model calculations of the specific heat in a system with two Einstein oscillators and an electronic contribution $C_{p,\mathrm{electronic}} = aT$. For the solid curve imposed on the $Ba_8Ga_{16}Ge_{30}$ data Einstein temperatures (θ_E) of 80 and 42 K were used and the numbers of Einstein atoms (N_E) were 6.5 per u.c. and 1.5 per u.c., respectively. The corresponding numbers for $Sr_8Ga_{16}Ge_{30}$ are $\theta_E = 80$ and 33 K, with $N_E = 6.5$ per u.c. and 1.5 per u.c., respectively. For the electronic contribution $a = 0.035$ and 0.04 J/(K^2 mol)/u.c. for $Ba_8Ga_{16}Ge_{30}$ and $Sr_8Ga_{16}Ge_{30}$, respectively. Dashed curves are Einstein contributions with $\theta_E = 33$, 42, and 80 K with $N_E = 1.5$ per u.c., 1.5 per u.c., and 6.5 per u.c., respectively. The inset shows the measured specific heat ($C_{p,\mathrm{meas}}$) of $Ba_8Ga_{16}Ge_{30}$ (circles) and $Sr_8Ga_{16}Ge_{30}$ (squares) as a function of temperature (T). The solid curve is the specific heat from a Debye model with 46 atoms per unit cell (u.c.) and a Debye temperature (θ_D) of 312 K ($C_{p,\mathrm{Debye}}$).

If θ_{E2} was to be related to the "normal" localized thermal vibration of the guest atoms, N_{E2} should be of the same order as the number of guest atoms in the unit cell. As the temperature increases the guest atoms are thermally exited into states where small anharmonic deviations on the potential floor have little influence. In this case θ_E obtained from the ADPs and high temperature $C_p(T)$ corresponds to those calculated in Ref. 18. It has been suggested that tunneling states, related to the off-center position of the guest atoms, exist in $Eu_8Ga_{16}Ge_{30}$ and $Sr_8Ga_{16}Ge_{30}$.[4,8,20,25] Recently also a specific four-well tunneling model for $Eu_8Ga_{16}Ge_{30}$ was proposed.[44] However, above it was argued that the potential in each cage must be slightly asymmetric due to the semirandom distribution of the framework elements. Furthermore, if the non-Debye and nonelectronic contribution to $C_p(T)$ is interpreted as a contribution from tunneling states, then the analysis of the low temperature $C_p(T)$ gives $N_{E2} \approx 1.5$ per u.c. for $Sr_8Ga_{16}Ge_{30}$ and $Ba_8Ga_{16}Ge_{30}$. This shows that the total number of states is too low to be related to the guest atoms in each of the large cages.

VI. MEM NUCLEAR DIFFERENCE DENSITIES

In the previous sections indirect evidence for the guest atom disorder in type I clathrates was obtained through analysis of refined ADPs. It is possible to obtain a direct verification of the disorder by analysis of the same data with the maximum entropy method (MEM). The MEM for analysis of accurate diffraction data has been extensively presented in the literature.[46] Initial MEM analysis of the $Ba_8Ga_{16}Si_{30}$ single crystal neutron data was presented in Ref. 24. Here we extend the analysis by calculating MEM nuclear *difference* densities at all temperatures. As before we have used the program MEED[47] with nonuniform prior (NUP) densities.[48] The NUPs were obtained by a structure factor aliasing method proposed by Roversi *et al.*[49] and implemented in the program ASF.[50] The NUPs were calculated with 28 structure factor copies and a cutoff value of 10^{-9}. In the present study the NUPs correspond to the nuclear densities of assemblies of ordered nuclei having anisotropic harmonic motion. Thus we have not biased the MEM calcula-

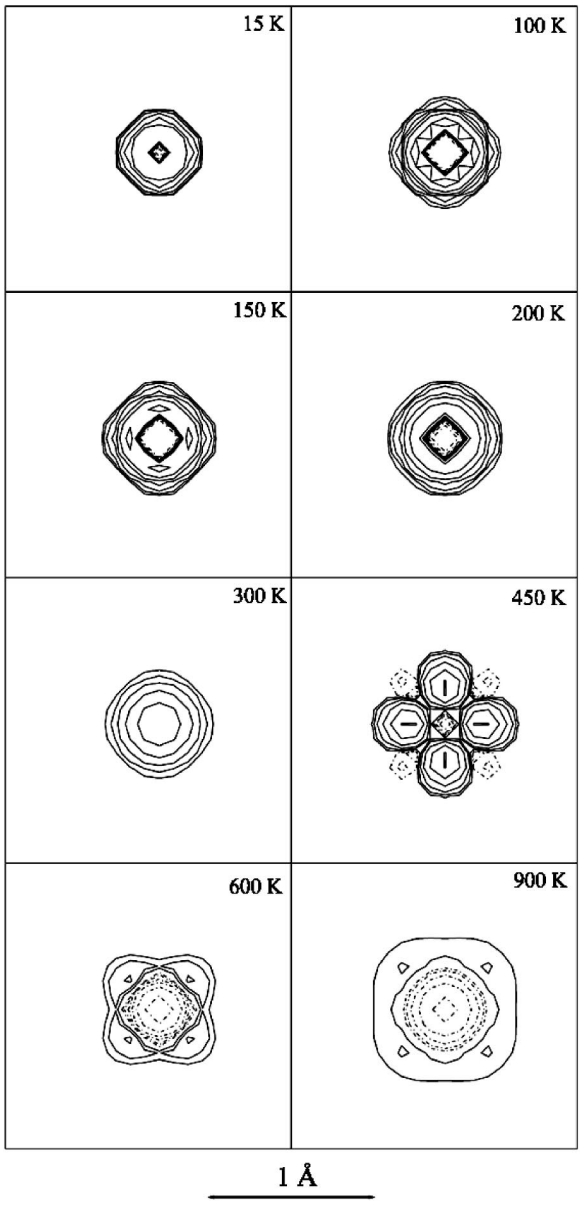

FIG. 7. MEM difference densities, $\rho(\mathrm{MEM}) - \rho(\mathrm{NUP})$, in the (001) plane through Ba(1) from 15 to 900 K. The difference densities are plotted on a logarithmic scale, 0.0125×2^N (n=0, …, 6), and solid contours are positive and dotted contours are negative.

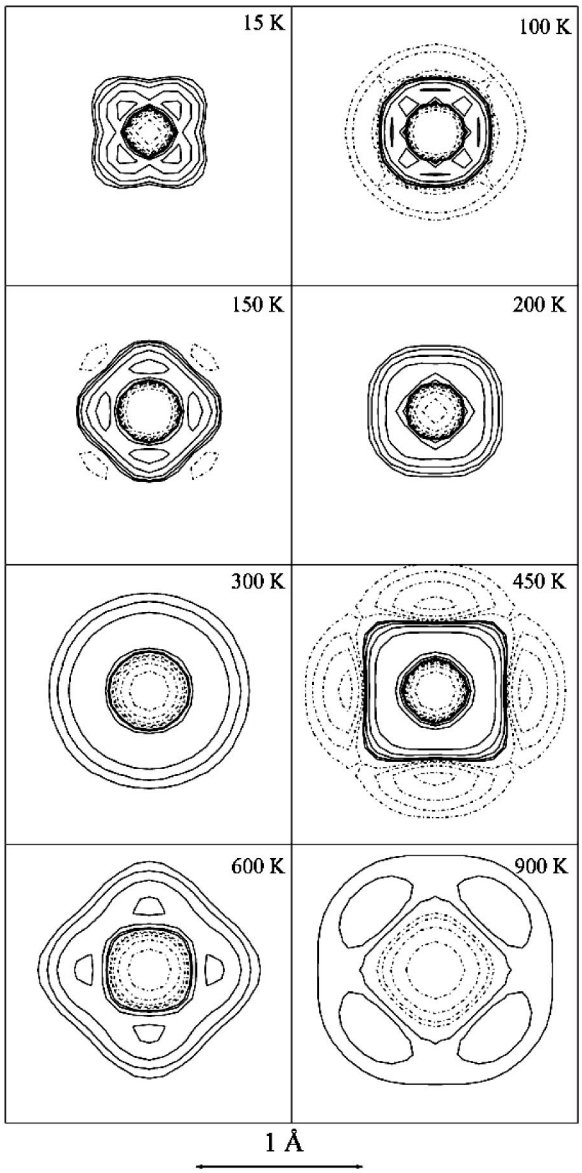

FIG. 8. MEM difference densities, ρ(MEM)$-\rho$(NUP), in the (100) plane through Ba(2) from 15 to 900 K. Contours as in Fig. 8.

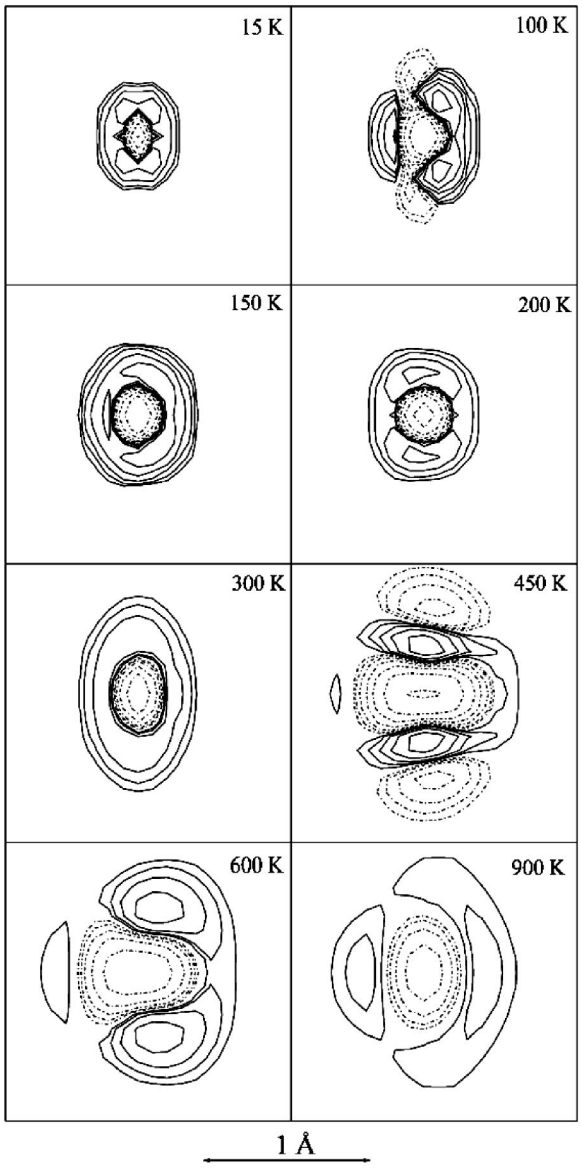

FIG. 9. MEM difference densities, ρ(MEM)$-\rho$(NUP), in the (001) plane through Ba(2) from 15 to 900 K. Contours as in Fig. 8.

tions with modeled anharmonicity from the conventional least-squares procedure. In all MEM calculations a $128\times128\times128$ pixel grid was used and iterations were stopped at $\chi^2=1$. The crystallographic *R*-factors corresponding to the final MEM densities are listed in Table VI. It should be stressed that the MEM calculations were not "difference" calculations, i.e., calculations based on structure factor differences ($\Delta F=F^{\mathrm{obs}}-F^{\mathrm{model}}$). They were "normal" total density calculations started from a NUP. Chakoumakos and coworkers have used nuclear densities extensively for discussion of disorder in thermoelectric clathrates.[21,22] In these studies straightforward nuclear densities for the guest atoms were obtained from Fourier analysis. For Ba2 in $Ba_8Ga_{16}Ge_{30}$ the nuclear density is broad, but centered at the center of the cage. One problem is that Fourier maps are prone to termination effects (ripples), and it is well established that MEM maps are superior to direct Fourier maps.[51] However, even in the MEM nuclear density there are no clear effects of disorder for $Ba_8Ga_{16}Si_{30}$ (see Fig. 2 of Ref. 24). In Figs. 7–9 MEM nuclear *difference* densities are shown for Ba1 and Ba2. These are not to be confused with the Fourier difference densities of Refs. 21 and 22, where model structure factors for part of a structure are subtracted from the observed structure factors in Fourier space. Our maps are calculated by subtraction of the NUPs from the final MEM density. The NUP is based on a model with structurally ordered guest atoms located in the centers of the cavities having anisotropic, harmonic thermal motion. For Ba2 there is at all temperatures a negative difference density in the center of the cavity surrounded by a positive region, Figs. 9 and 10. Since we do not expect extensive anharmonic motion at 15 K, the low temperature features around Ba2 in the difference density must be interpreted as structural disorder. The features appearing in the difference density above room temperature can be ascribed to anharmonic effects. The an-

isotropic thermal parameters used in the NUP may limit the resolving power of the difference density by modeling some guest atom disorder. However, had we used isotropic thermal parameters in the NUP, anisotropic motion would be superimposed on the structural disorder, and the difference density features would be difficult to assign as structural disorder. When the anisotropic NUP is different from the final MEM at the lowest temperature, it is a strong (conservative) evidence of disorder. The MEM difference densities suggest that the Ba2 disorder is temperature dependent with the negative central area increasing in size at higher temperatures. This means that on average the guest atoms are located farther from the cage center at high temperatures. The small peak maxima in the positive distribution changes direction from temperature to temperature, and shows directly the almost equivalence between the 24*j* and 24*k* disorder sites. The true disorder position is probably represented by a cylindrical volume. Note that the excessive (ghost) features observed at 450 K once again illustrate the relatively poorer quality of this data set. For Ba1 the difference density features are less pronounced, but basically follow the same trend as for Ba2. The MEM nuclear difference density reveals structural disorder on the Ba1 site possibly with onset of anharmonic motion above room temperature. Figures 7–9 clearly illustrate that the resolving power of difference densities is higher than for normal nuclear densities.[24] This is a well-known result in crystallography. In x-ray charge density analysis various types of deformation densities are commonly used for enhancing subtle electronic details (e.g., orbital hybridization, lone pairs, covalent bonding, etc.).[52] We have previously reported MEM difference electron densities for $Sr_8Ga_{16}Ge_{30}$ and $Ba_8Ga_{16}Ge_{30}$.[7] Nuclear difference densities are the logical extensions of such analysis to problems of subtle structural disorder.

VII. CONCLUSION

The structural properties of $Ba_8Ga_{16}Si_{30}$, $Ba_8Ga_{16}Ge_{30}$, $Ba_8In_{16}Ge_{30}$, and $Sr_8Ga_{16}Ge_{30}$ have been investigated by synchrotron and neutron diffraction. It has been shown that the temperature dependence of the framework ADPs can be described well with a Debye model if a temperature independent disorder parameter is included. The magnitude of *d* describes variation of the equilibrium position due to the semirandom positioning of the framework atoms. *d* increases with increasing variation of the framework covalent bond lengths. Similarly, an Einstein model with a temperature independent *d* has been used for describing the temperature dependence of the guest atom ADPs. It has been shown that *none* of the guest atoms in the large cages are located in the center. This conclusion is corroborated by MEM nuclear difference density maps.

Application of an Einstein model for the guest atoms indicates that θ_E for all vibrational modes of Sr in $Sr_8Ga_{16}Ge_{30}$ is larger than for Ba in any of the Ba containing clathrates. This is somewhat surprising due to the large ADPs observed for Sr, but nonetheless in good agreement with theoretical predictions. Comparison of the ADP results with theory and $C_p(T)$ data shows that θ_E obtained from the ADPs are related to vibrations in the full potential formed by the cages. However, smaller θ_E values from $C_p(T)$ have been reported in the literature relative to values obtained by theory and the ADPs. We have therefore reinvestigated the low temperature $C_p(T)$ of $Ba_8Ga_{16}Ge_{30}$ and $Sr_8Ga_{16}Ge_{30}$. The new analysis shows that a nonelectronic and non-Debye contribution to $C_p(T)$ is present. The density of states is localized with a characteristic energy of approximately 35 K. The total number of states is around 1 state per u.c. and this is too small to be directly related to vibrations in the potential formed by the cages. Instead we suggest that it is related to nonharmonic features at the bottom of the potential well.

ACKNOWLEDGMENTS

We gratefully acknowledge the beam time obtained at the SCD station at the Intense Pulsed Neutron Source, Argonne National Laboratory. The SCD is supported by the U. S. DOE-BES under Contract No. W-31-109-ENG-30. Dr. Arthur Schultz, Dr. R. W. Henning, and Dr. M. E. Miller are thanked for assistance with the data collection. We thank the Japanese Synchrotron Radiation Institute for granting beam time at SPring8, and Professor Masaki Takata and Professor Makoto Sakata are thanked for fruitful discussions. Dr. Dan Bryan is thanked for supplying some of the samples.

*Corresponding author. FAX: +45-8619 6199. Email address: bo@chem.au.dk

[1] F. J. DiSalvo, Science **285**, 703 (1999).
[2] G. A. Slack, in *CRC Handbook of Thermoelectrics*, edited by D. M. Rowe (CRC Press, Boca Raton, Fl., 1995), p. 407.
[3] G. S. Nolas, J. L. Cohn, G. A. Slack, and S. B. Schujman, Appl. Phys. Lett. **73**, 178 (1998).
[4] J. L. Cohn, G. S. Nolas, V. Fessatidis, T. H. Metcalf, and G. A. Slack, Phys. Rev. Lett. **82**, 779 (1999).
[5] B. B. Iversen, A. E. C. Palmqvist, D. E. Cox, G. S. Nolas, G. D. Stucky, N. P. Blake, and H. Metiu, J. Solid State Chem. **149**, 455 (2000).
[6] V. L. Kuznetsov, L. A. Kuznetsova, A. E. Kaliazin, and D. M. Rowe, J. Appl. Phys. **87**, 7871 (2000).
[7] A. Bentien, A. E. C. Palmqvist, J. D. Bryan, S. Latturner, G. D. Stucky, L. Furenlid, and B. B. Iversen, Angew. Chem., Int. Ed. **39**, 3613 (2000).
[8] B. C. Sales, B. C. Chakoumakos, R. Jin, J. R. Thompson, and D. Mandrus, Phys. Rev. B **63**, 245113 (2001).
[9] S. Paschen, W. Carrillo-Cabrera, A. Bentien, V. H. Tran, M. Baenitz, Y. Grin, and F. Steglich, Phys. Rev. B **64**, 214404 (2001).
[10] J. D. Bryan, N. P. Blake, H. Metiu, G. D. Stucky, B. B. Iversen, R. D. Poulsen, and A. Bentien, J. Appl. Phys. **92**, 7281 (2002); **93**, 4343(E) (2003).
[11] Y. Mudryk, P. Rogl, C. Paul, S. Berger, E. Bauer, G. Hilscher, C.

Godart, and H. Noël, J. Phys.: Condens. Matter **14**, 7991 (2002).
[12] H. Schäfer, Annu. Rev. Mater. Sci. **15**, 1 (1985).
[13] C. Gatti, L. Bertini, N. P. Blake, and B. B. Iversen, Chem.-Eur. J. **9**, 4556 (2003).
[14] J. S. Tse and M. A. White, J. Phys. Chem. **92**, 5006 (1988).
[15] J. J. Dong, O. F. Sankey, and C. W. Myles, Phys. Rev. Lett. **86**, 2361 (2001).
[16] B. Eisenmann, H. Schäfer, and R. Zagler, J. Less-Common Met. **118**, 43 (1986).
[17] B. Kuhl, A. Czybulka, and H. U. Schuster, Z. Anorg. Allg. Chem. **621**, 1 (1995).
[18] N. P. Blake, D. Bryan, S. Latturner, L. Møllnitz, G. D. Stucky, and H. Metiu, J. Chem. Phys. **114**, 10063 (2001).
[19] D. Nataraj, J. Nagao, M. Ferhat, and T. Ebinuma, J. Appl. Phys. **93**, 2424 (2003).
[20] V. Keppens, M. A. McGuire, A. Teklu, C. Laermans, B. C. Sales, D. Mandrus, and B. C. Chakoumakos, Physica B **316**, 95 (2002).
[21] B. C. Chakoumakos, B. C. Sales, D. G. Mandrus, and G. S. Nolas, J. Alloys Compd. **296**, 80 (2000).
[22] B. C. Chakoumakos, B. C. Sales, and D. G. Mandrus, J. Alloys Compd. **322**, 127 (2001).
[23] B. B. Iversen, A. Bentien, A. E. C. Palmqvist, J. D. Bryan, and G. D. Stucky, in *Proceedings of the 19th International Conference on Thermoelectrics*, edited by D. M. Rowe (BABROW Press, Wales, UK, 2000), p. 113.
[24] A. Bentien, B. B. Iversen, J. D. Bryan, G. D. Stucky, A. E. C. Palmqvist, A. J. Schultz, and R. W. Henning, J. Appl. Phys. **91**, 5694 (2002).
[25] V. Keppens, B. C. Sales, D. Mandrus, B. C. Chakoumakos, and C. Laermans, Philos. Mag. Lett. **80**, 807 (2000).
[26] A. Bentien, M. Christensen, J. D. Bryan, A. Sanchez, S. Paschen, F. Steglich, G. D. Stucky, and B. Iversen, Phys. Rev. B **69**, 045107 (2004).
[27] F. Tournus, B. Masenelli, P. Mélinon, D. Connétable, X. Blase, A. M. Flank, P. Legarde, C. Cros, and M. Pouchard, Phys. Rev. B **69**, 035208 (2004).
[28] J. D. Bryan, *Dissertation in Chemistry* (University of California, Santa Barbara, 2002).
[29] A. J. Schultz, K. Srinivasan, R. G. Teller, J. M. Williams, and C. M. Lukehart, J. Am. Chem. Soc. **106**, 999 (1984).
[30] V. F. Sears, Neutron News **3**, 26 (1992).
[31] E. Nishibori, M. Takata, K. Kato, M. Sakata, Y. Kubota, S. Aoyagi, Y. Kuroiwa, M. Yamakata, and N. Ikeda, Nucl. Instrum. Methods Phys. Res. A **467**, 1045 (2001).
[32] A. C. Larson, Los Alamos National Laboratory Report No. LAUR 86-748, 2000 (unpublished).
[33] N. Lock, M. Christensen, A. J. Schultz, and B. B. Iversen (unpublished).
[34] V. Pacheco, A. Bentien, W. Carrillo-Cabrera, S. Paschen, F. Steglich, and Y. Grin, Phys. Rev. B (to be published April 2005).
[35] A. Bentien, V. Pacheco, S. Paschen, Y. Grin, and F. Steglich, Phys. Rev. B (to be published April 2005).
[36] R. H. Blessing, J. Appl. Crystallogr. **30**, 421 (1997).
[37] T. Koritzansky, S. T. Howard, M. P. R. Z. Su, T. Richter, and N. K. Hansen (unpublished).
[38] B. T. M. Willis and A. W. Pryor, *Thermal Vibrations in Crystallography* (Cambridge University Press, London, 1975).
[39] B. B. Iversen, S. K. Nielsen, and F. K. Larsen, Philos. Mag. A **72**, 1357 (1995).
[40] D. Sledziew and A. Rajca, J. Phys. Chem. Solids **35**, 181 (1974).
[41] Y. G. Zhang, P. L. Lee, G. S. Nolas, and A. P. Wilkinson, Appl. Phys. Lett. **80**, 2931 (2002).
[42] B. B. Iversen, F. K. Larsen, B. N. Figgis, P. A. Reynolds, and A. J. Schultz, Acta Crystallogr., Sect. B: Struct. Sci. **52**, 923 (1996).
[43] H. B. Burgi and S. C. Capelli, Acta Crystallogr., Sect. A: Found. Crystallogr. **56**, 403 (2000).
[44] I. Zerec, V. Keppens, M. A. McGuire, D. Mandrus, B. C. Sales, and P. Thalmeier, Phys. Rev. Lett. **92**, 185502 (2004).
[45] G. S. Nolas and C. A. Kendziora, Phys. Rev. B **62**, 7157 (2000).
[46] M. Takata, E. Nishibori, and M. Sakata, Z. Kristallogr. **216**, 71 (2001).
[47] S. Kumazawa, Y. Kubota, M. Takata, M. Sakata, and Y. Ishibashi, J. Appl. Crystallogr. **26**, 453 (1993).
[48] B. B. Iversen, F. K. Larsen, M. Souhassou, and M. Takata, Acta Crystallogr., Sect. B: Struct. Sci. **51**, 580 (1995).
[49] P. Roversi, J. J. Irwin, and G. Bricogne, Acta Crystallogr., Sect. A: Found. Crystallogr. **54**, 971 (1998).
[50] A. Bentien, Thesis for the Masters Degree, Department of Chemistry, University of Aarhus, 2000 (unpublished).
[51] M. Sakata and M. Sato, Acta Crystallogr., Sect. A: Found. Crystallogr. **46**, 263 (1990).
[52] P. Coppens, *X-ray Charge Densities and Chemical Bonding* (Oxford University Press, New York, 1997).